Multivariate sodalite Zeolitic Imidazolate frameworks: a direct solvent-free synthesis

Javier López-Cabrelles,[a] Eugenia Miguel-Casañ,[a] María Esteve-Rochina,[a] Eduardo Andres-Garcia,[a] Iñigo J. Vitórica-Yrezábal,[b]Joaquín Calbo,[a] and Guillermo Mínguez Espallargas[a] *

[a] *Instituto de Ciencia Molecular (ICMol), Universidad de Valencia, c/Catedrático José Beltrán, 2, 46980 Paterna, Spain*

[b] *School of Chemistry, University of Manchester, Oxford Road, Manchester M13 9PL (United Kingdom)*

Supporting Information

Contents

S1. Synthesis of mixed-ligand ZIFs 2
S2. Characterization of Mixed-ligand ZIFs 2
S2.1 X-ray powder diffraction 2
S.2.1.1 Mixture 2-methylimidazole and 2-ethylimidazole (miH/eiH) 3
S.2.1.2 Pure ligands synthesis 4
S2.2 Single-crystal diffraction 6
S2.3 Magnetic properties 9
S2.4 NMR studies 11
S2.5 Thermal stability 19
S2.6 Infrared spectroscopy 22
S2.7 Scanning electron microscopy 24
S2.8 N_2 and CO_2 gas sorption 26
S3 Theoretical calculations 29
S4 Water stability characterization 35
S4.1 X-ray powder diffraction 36
S4.2 NMR spectroscopy 38
S4.3 Contact angle measurements 42
S5 References 43

S1. Synthesis of mixed-ligand ZIFs

All reagents were commercially available and used without further purification.

Synthesis of MUV-3-eimb and **MUV-3-mimb.** Ferrocene (30 mg, 0.16 mmol) and a combination of 2-methylimidazole, 2-ethylimidazole and/or 2-methylbenzimidazole (0.10-0.24 mmol per reactant) were combined and sealed under vacuum in a layering tube (4 mm diameter). The mixture was heated at 150 °C for 4 days to obtain yellow crystals suitable for X-ray single-crystal diffraction. The product was allowed to cool to room temperature, and the layering tube was then opened. The unreacted precursors were extracted with acetonitrile and benzene, and **MUV-3-eimb** and **MUV-3-mimb** were isolated as yellow crystals. Phase purity was established by X-ray powder diffraction.

Synthesis of ZIF-8-eimb, **ZIF-8-mimb**, **ZIF-8-eimi, ZIF-67-eimb**, **ZIF-67-mimb, ZIF-67-eimi**. Cobaltocene (for ZIF-67-mix, 30 mg, 0.16 mmol) or ZnO (for ZIF-8-mix, 13 mg, 0.16 mmol) and a combination of 2-methylimidazole, 2-ethylimidazole and/or 2-methylbenzimidazole (0.10-0.24 mmol per reactant) were combined and sealed under vacuum in a layering tube (4 mm diameter). The mixtures were heated at 150 °C for 4 days to obtain purple powder (**ZIF-67-eimb**, **ZIF-67-mimb, ZIF-67-eimi**) or white powder (**ZIF-8-eimb**, **ZIF-8-mimb**, **ZIF-8-eimi**). The products were allowed to cool to room temperature, and the layering tubes were then opened. The unreacted precursors were extracted with acetonitrile and benzene. Phase purity was established by X-ray powder diffraction.

S2. Characterization of Mixed-ligand ZIFs

S2.1 X-ray powder diffraction

Polycrystalline samples of mixed ligand ZIFs **ZIF-8-eimb**, **ZIF-8-mimb**, **ZIF-8-eimi, ZIF-67-eimb**, **ZIF-67-mimb, ZIF-67-eimi, MUV-3-eimb**, and **MUV-3-mimb**, and pure ligands ZIFs **ZIF-8, Zn(ei)$_2$, Zn(mb)$_2$, ZIF-67, Co(ei)$_2$, Co(mb)$_2$, MUV-3, MUV-6** and **MUV-7** (prepared by solvent-free synthesis) were lightly ground in an agate mortar and pestle and used to fill 0.5 mm borosilicate capillaries that were mounted and aligned on an Empyrean PANalytical powder diffractometer, using Cu Kα radiation (λ = 1.54056 Å). Three repeated measurements were collected at room temperature (2θ = 2−40 °) and merged in a single diffractogram for each sample, with sharp and intense peaks denoting the high crystallinity of the material.

S.2.1.1 Mixture 2-methylimidazole and 2-ethylimidazole (miH/eiH)

For the Fe(II) mixture, only the presence of segregated phases was observed. Compared with the **MUV-3** pattern, the presence of SOD material was not found. For Co(II) and Zn(II), only one crystalline phase was observed, matching in great agreement with the SOD diffraction pattern.

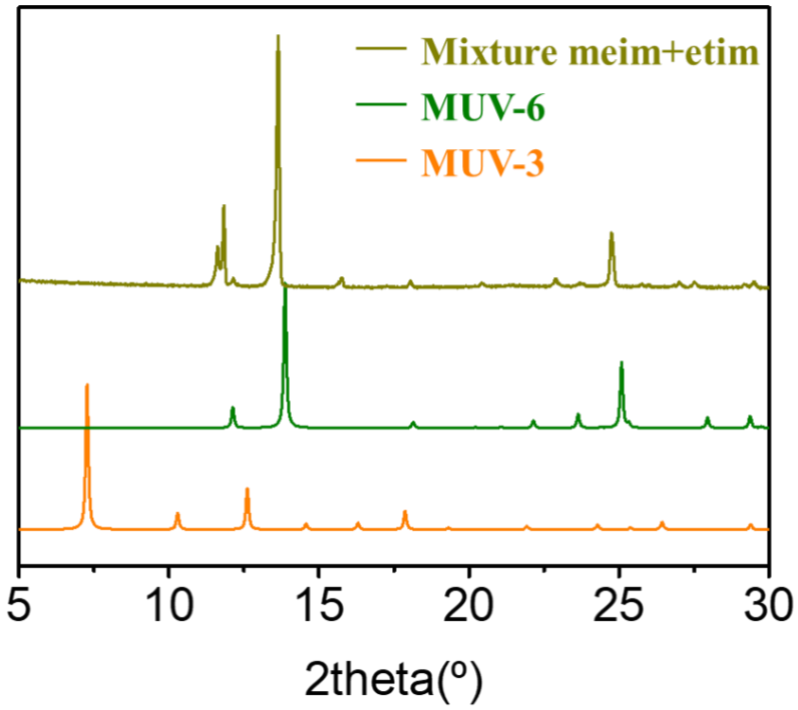

Figure S1. X-ray powder diffraction patterns of the obtained material for Fe(II) and the mixture miH/eiH.

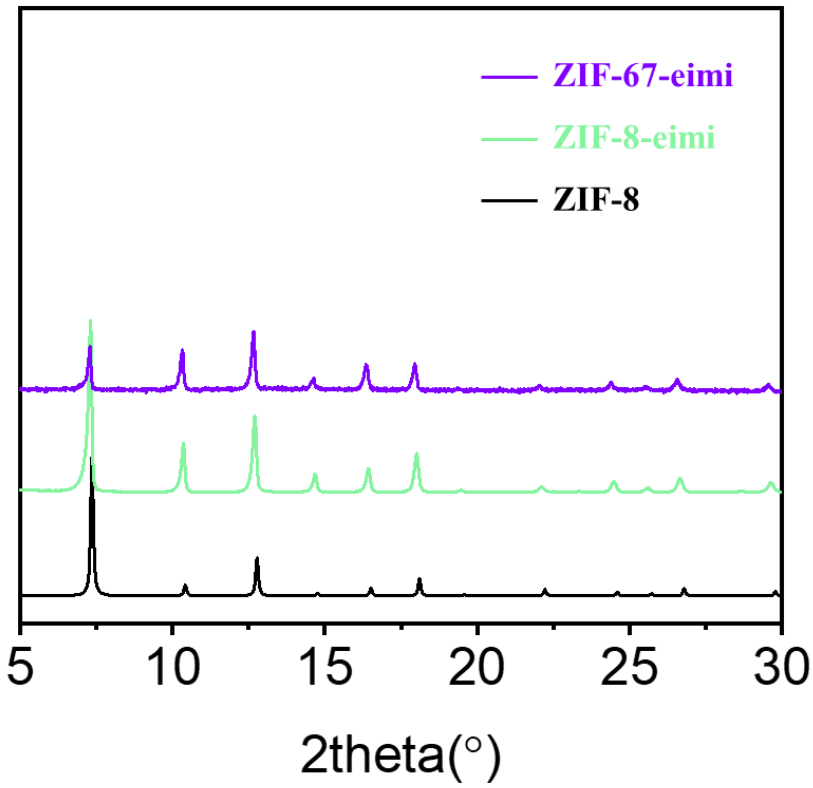

Figure S2. X-ray powder diffraction patterns of the obtained material for Co(II) and Zn(II) with the mixture mi/ei.

S.2.1.2 Pure ligands synthesis

For the Fe(II) compounds, the obtained pure ligand structures are reported by the group previously.[1] For Zn(II) and Co(II), several crystal phases were found.

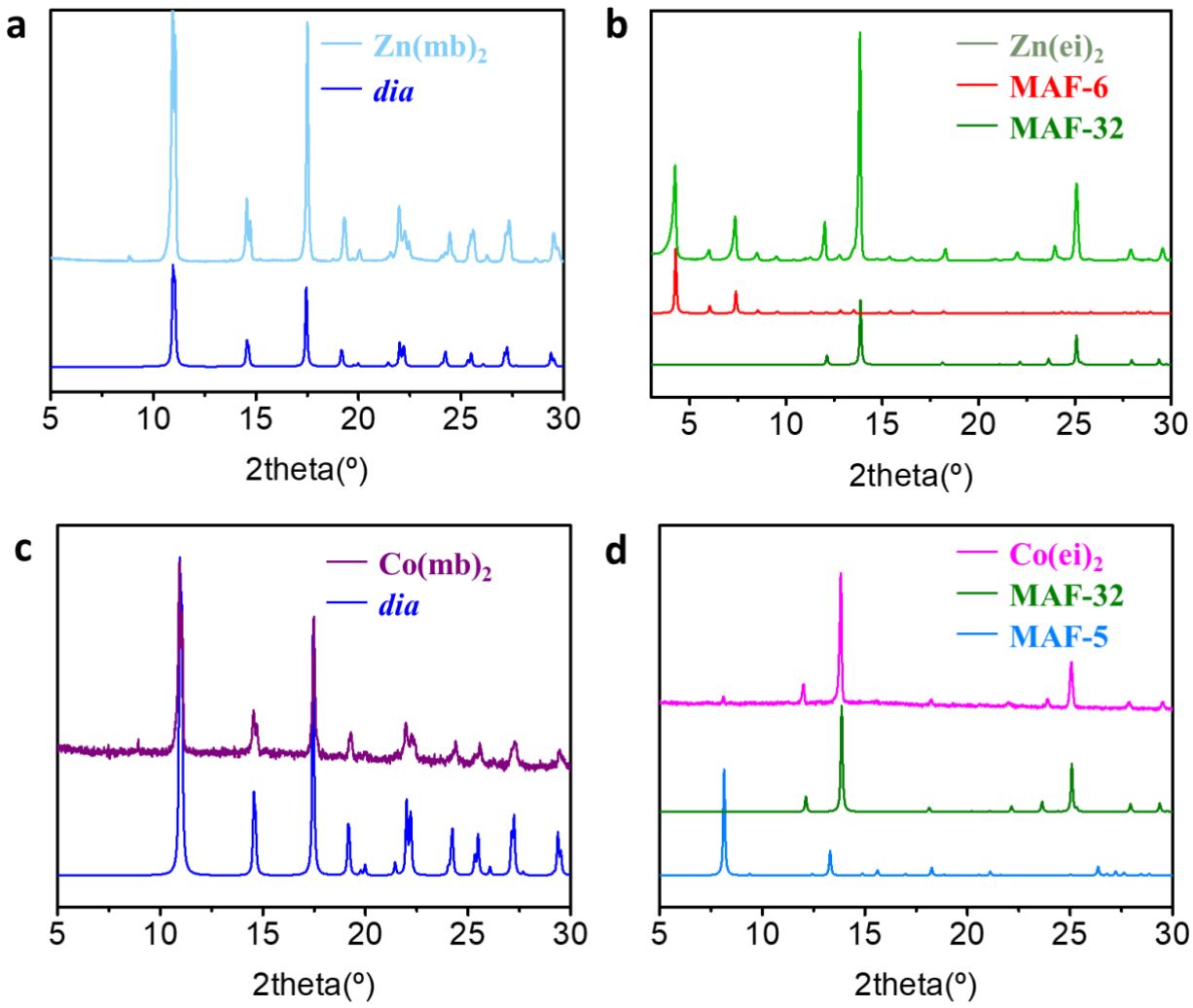

Figure S3. a) X-ray powder diffraction pattern of $Zn(mb)_2$, showing the ***dia*** topology. b) X-ray powder diffraction pattern of $Zn(ei)_2$ presenting the ***qtz*** (MAF-32) and RHO (MAF-6) topologies. c) X-ray powder diffraction pattern of $Co(mb)_2$ showing the ***dia*** topology. d) The X-ray powder diffraction pattern of $Co(ei)_2$ is a mixture of two very known structures, small amount of MAF-5 (ANA) and MAF-32 (***qtz***). The theoretical ***dia*** patterns are extracted from the **MUV-7** single crystal data.

S2.2 Single-crystal diffraction

Single crystals of **MUV-3-eimb** and **MUV-3-mimb** were mounted on cryoloops using a viscous hydrocarbon oil to coat the crystals. X-ray data were collected at 120 K on a Supernova diffractometer equipped with a graphite-monochromated Enhance (Mo) X-ray Source ($\lambda = 0.71073$ Å). The program CrysAlisPro, Oxford Diffraction Ltd., was used for unit cell determinations and data reduction. Empirical absorption correction was performed using spherical harmonics, implemented in the SCALE3 ABSPACK scaling algorithm. Crystal structures were solved and refined against all F^2 values by using the SHELX and Olex2 suite of programs.[2,3] Non-hydrogen atoms were refined anisotropically and hydrogen atoms were placed at calculated positions (riding model).

Both crystal structures had deformed electron density remaining in the pores. Solvent Mask implemented in OLEX 2 resulted with 8 and 10 electrons for **MUV-3-eimb** and **MUV-3-mimb,** which corresponds to 1 molecule of water per asymmetric unit.

Disorder between the 2-methylbenzimidazolate (mb) and 2-methylimidazolate (mi) ligands in crystal structure **MUV-3-mimb** were refined and found to be 24.9/75.1 for mb/mi. Finally the occupancies were fixed to 25/75.

Disorder between the 2-methylbenzimidazolate (mb) and 2-ethylimidazolate (ei) ligands in crystal structure **MUV-3-eimb** were refined and found to be 32.9/67.1 for mb/ei. Finally the occupancies were fixed to 33/67.

CCDC 2095300-2095301 contains the supplementary crystallographic data for this paper. These data can be obtained free of charge via www.ccdc.cam.ac.uk/conts/retrieving.html (or from the Cambridge Crystallographic Data Centre, 12 Union Road, Cambridge CB21EZ, UK; fax: (+44)1223-336-033; or deposit@ccdc.cam.ac.uk).

Table S1. Crystallographic information for **MUV-3-eimb** and **MUV-3mimb**

Identification code	**MUV-3-eimb**	**MUV-3mimb**
Empirical formula	$C_{12}H_{14}FeN_4$	$C_{10}H_{11}FeN_4$
Formula weight	270.12	243.08
Temperature/K	120.00(10)	119.5(8)
Crystal system	cubic	cubic
Space group	I-43m	I-43m
a/Å	17.31700(10)	17.1728(6)
b/Å	17.31700(10)	17.1728(6)
c/Å	17.31700(10)	17.1728(6)
α/°	90	90
β/°	90	90
γ/°	90	90
Volume/Å^3	5193.00(9)	5064.3(6)
Z	12	12
ρ_{calc}g/cm^3	1.037	0.956
μ/mm^{-1}	0.858	0.874
F(000)	1680.0	1500.0
Crystal size/mm^3	0.18 × 0.16 × 0.15	0.17 × 0.16 × 0.16
Radiation	Mo Kα (λ = 0.71073)	Mo Kα (λ = 0.71073)
2Θ range for data collection/°	6.654 to 55.92	5.81 to 49.93
Index ranges	$-21 \le h \le 21$, $-22 \le k \le 21$, $-22 \le l \le 22$	$-20 \le h \le 20$, $-20 \le k \le 20$, $-20 \le l \le 20$
Reflections collected	33960	29016
Independent reflections	1169 [R_{int} = 0.0450, R_{sigma} = 0.0166]	863 [R_{int} = 0.1646, R_{sigma} = 0.0412]
Data/restraints/parameters	1169/8/65	863/39/56
Goodness-of-fit on F^2	1.008	1.041
Final R indexes [I>=2σ (I)]	R_1 = 0.0317, wR_2 = 0.0908	R_1 = 0.0538, wR_2 = 0.1108
Final R indexes [all data]	R_1 = 0.0482, wR_2 = 0.0980	R_1 = 0.0745, wR_2 = 0.1187
Largest diff. peak/hole / e Å^{-3}	0.21/-0.15	0.25/-0.26
Flack parameter	0.16(4)	0.12(8)

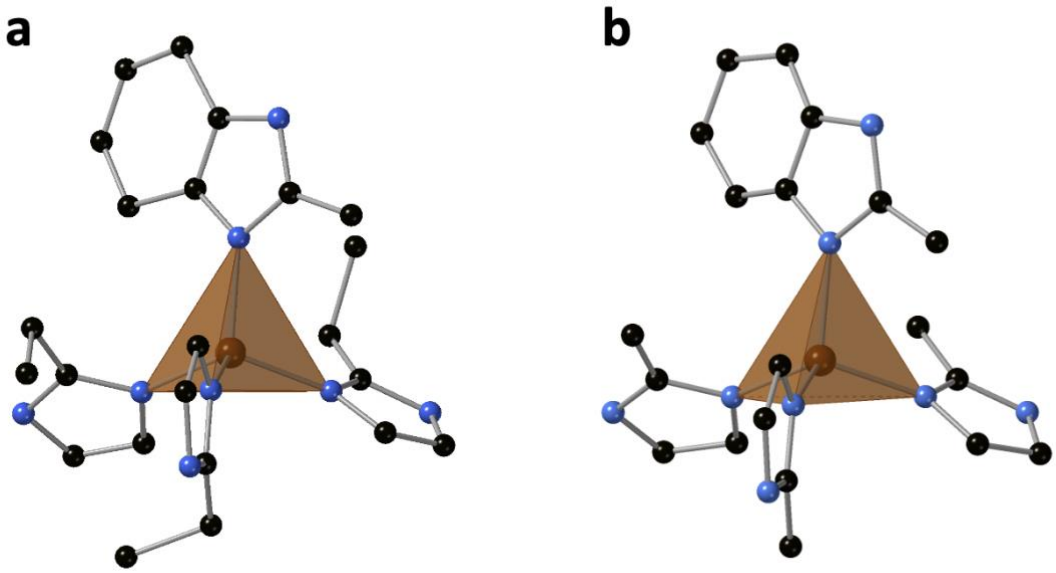

Figure S4. Coordination environment of the Fe(II) atoms in **MUV-3-eimb** (a) and **MUV-3-mimb** (b).

Table S2. Fe-N bonds distances in the different Fe(II)-azolates-based materials.

	MUV-3	**MUV-3-eimb**	**MUV-3-mimb**	**MUV-6**	**MUV-7**
Fe–N	2.0342 Å	2.0426 Å	2.0523 Å	2.0554–2.1787 Å	2.0404–2.0479 Å
a	17.1656 Å	17.2998 Å	17.1728 Å	-	-

S2.3 Magnetic properties

The magnetic structure and the presence of Fe(II) and Co(II) were characterized by magnetic measurements. Variable-temperature (2−300 K) direct current (dc) magnetic susceptibility measurements were carried out in applied fields of 0.1 T. The Neel temperatures were calculated following the Fisher criteria.[4] The T_N for the mixed-ligand materials are closer to the **MUV-3** (20.6 K) than the pure ligand compounds, which present different topologies (**MUV-6** and **MUV-7**). The structures which are composed by 2-methylbenzimidazolate present lower T_N for Fe(II) and Co(II) materials than the pure 2-methylimidazolate SOD compounds.

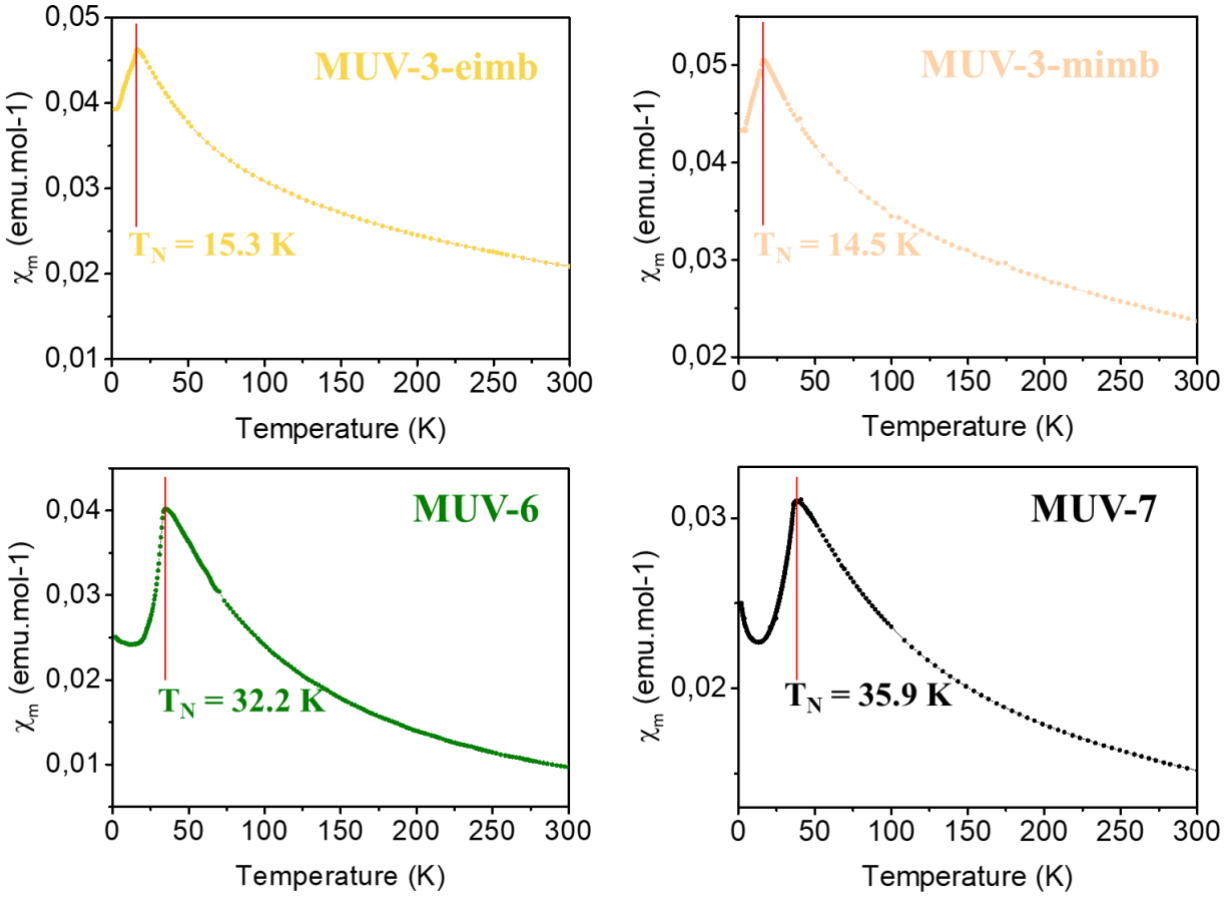

Figure S5. Magnetic susceptibility plot showing the antiferromagnetic interactions and antiferromagnetic ordering at low temperature between Fe(II) centers in **MUV-3-eimb**, **MUV-3-mimb**, **MUV-6** and **MUV-7.**

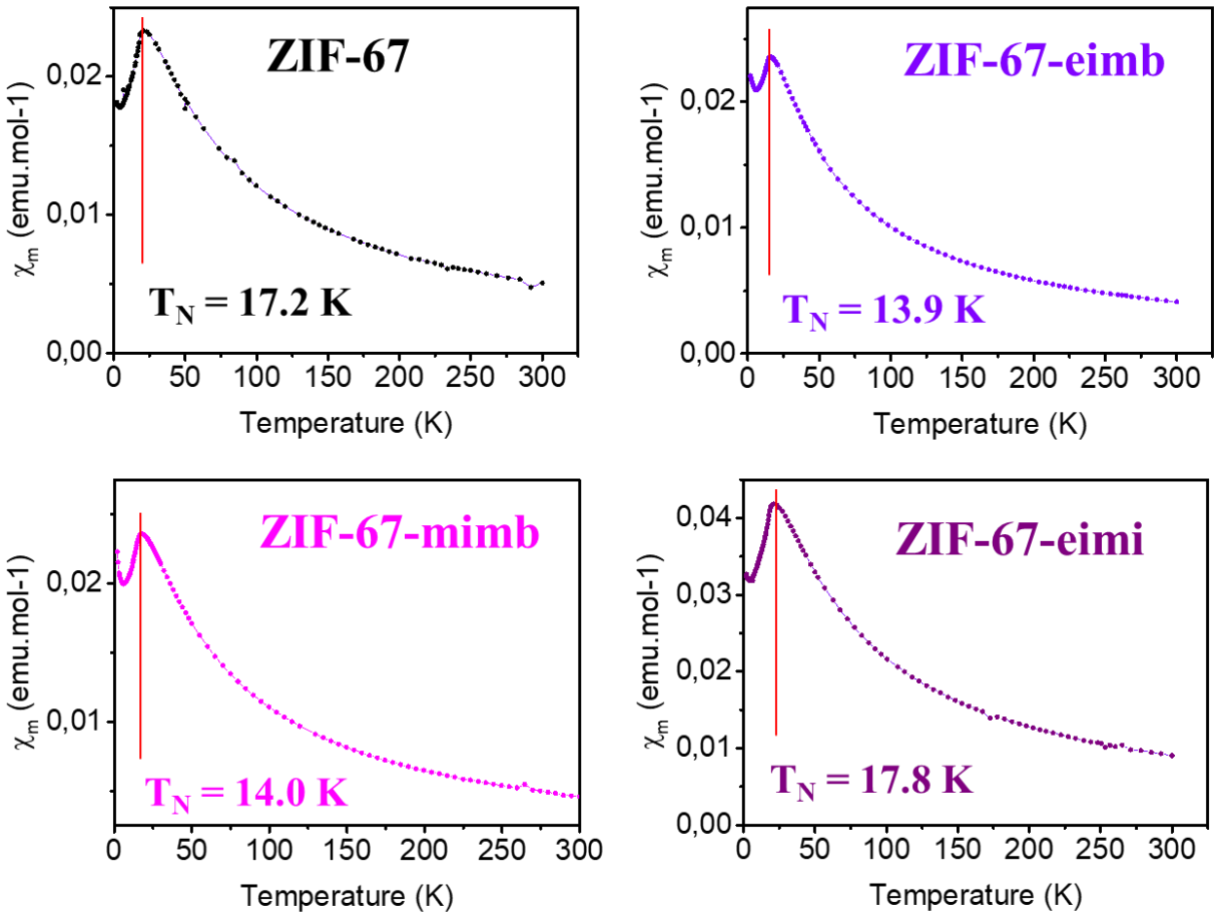

Figure S6. Magnetic susceptibility plot showing the antiferromagnetic interactions and antiferromagnetic ordering at low temperature between Co(II) centers in **ZIF-67**, **ZIF-67-eimb**, **ZIF-67-mimb** and **ZIF-67-eimi.**

S2.4 NMR studies

NMR spectra were recorded on Bruker DRX-500 spectrometer. The ligand ratio was confirmed by ^{1}H NMR spectroscopy (upon digestion in D_2O and deuterated trifluoroacetic acid for the comparison with the pure organic spectra) and ^{13}C NMR solid state spectroscopy (for **ZIF-8-eimb**, **ZIF-8-mimb** and **ZIF-8-eimi)**.

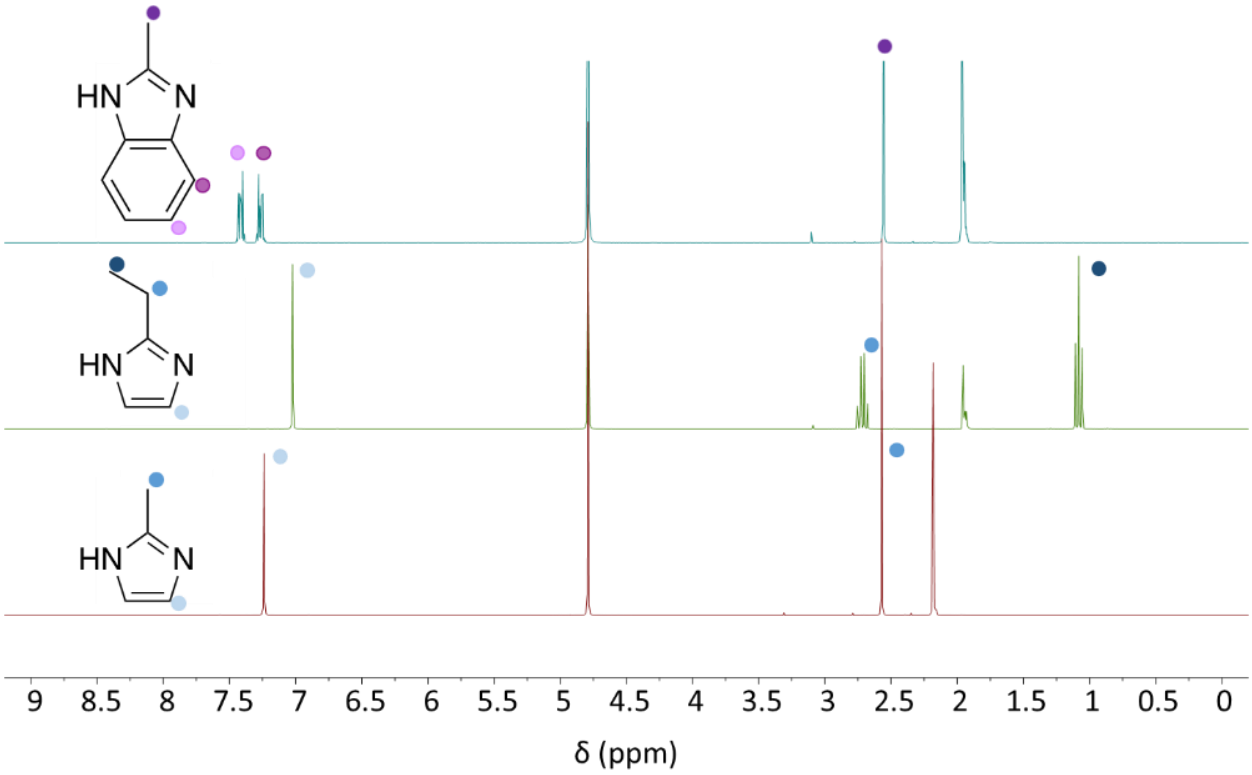

Figure S7. ^{1}H NMR spectra of the pure organic ligands used to construct the mixed-ligand ZIFs family. Coloured circles help to localize the corresponding chemical shifts of the protons.

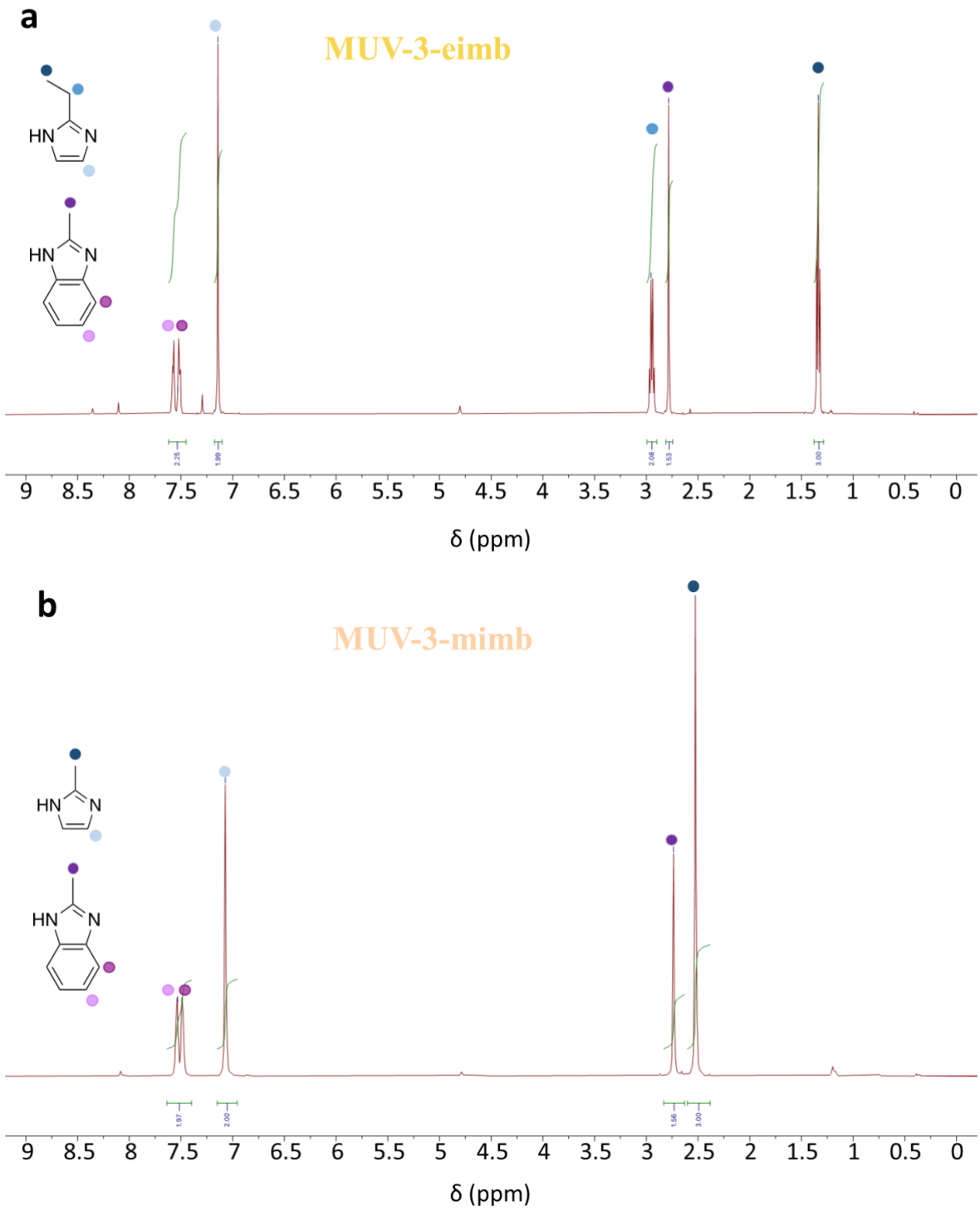

Figure S8. ^{1}H NMR spectra of digested **MUV-3-eimb** and **MUV-3-mimb**, where it can be clearly identified the H atoms from each ligand. Coloured circles help to localize the corresponding chemical shifts of the protons.

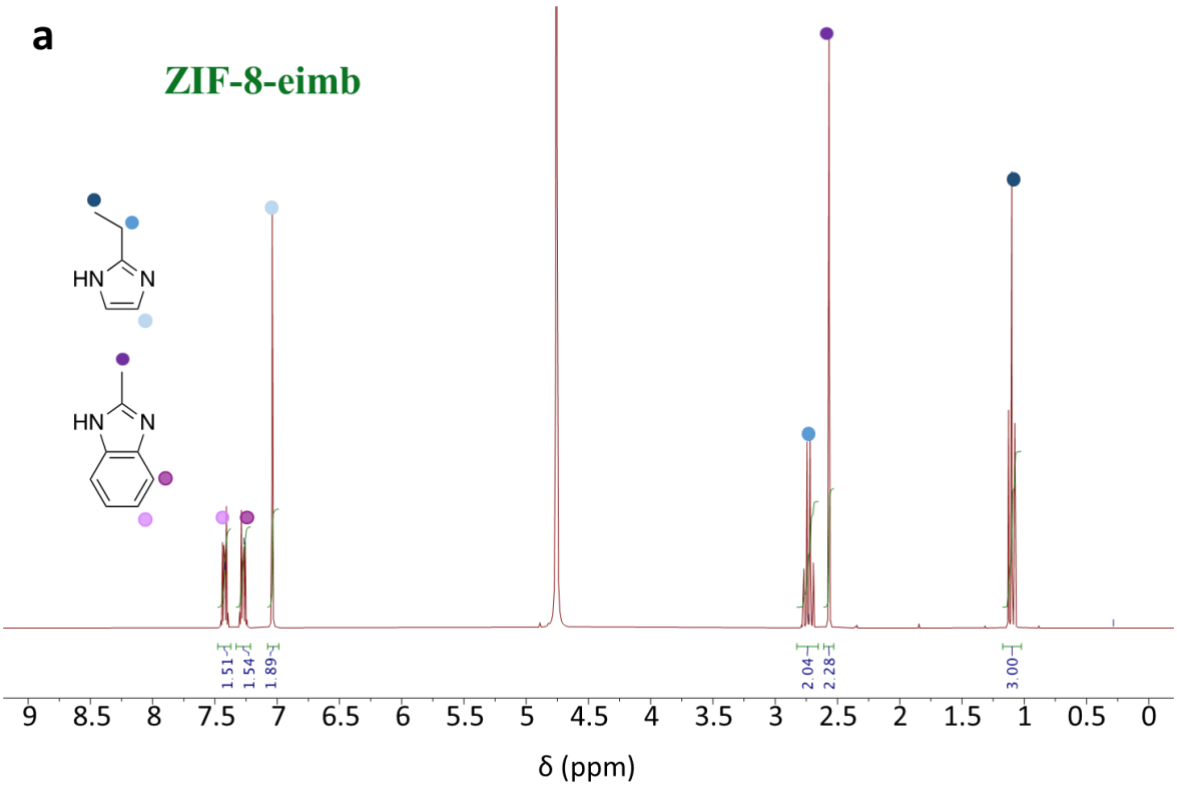
a
ZIF-8-eimb
HN
N
HN
N
1.51
1.54
1.89
2.04
2.28
3.00
9
8.5
8
7.5
7
6.5
6
5.5
5
4.5
4
3.5
3
2.5
2
1.5
1
0.5
0
δ (ppm)

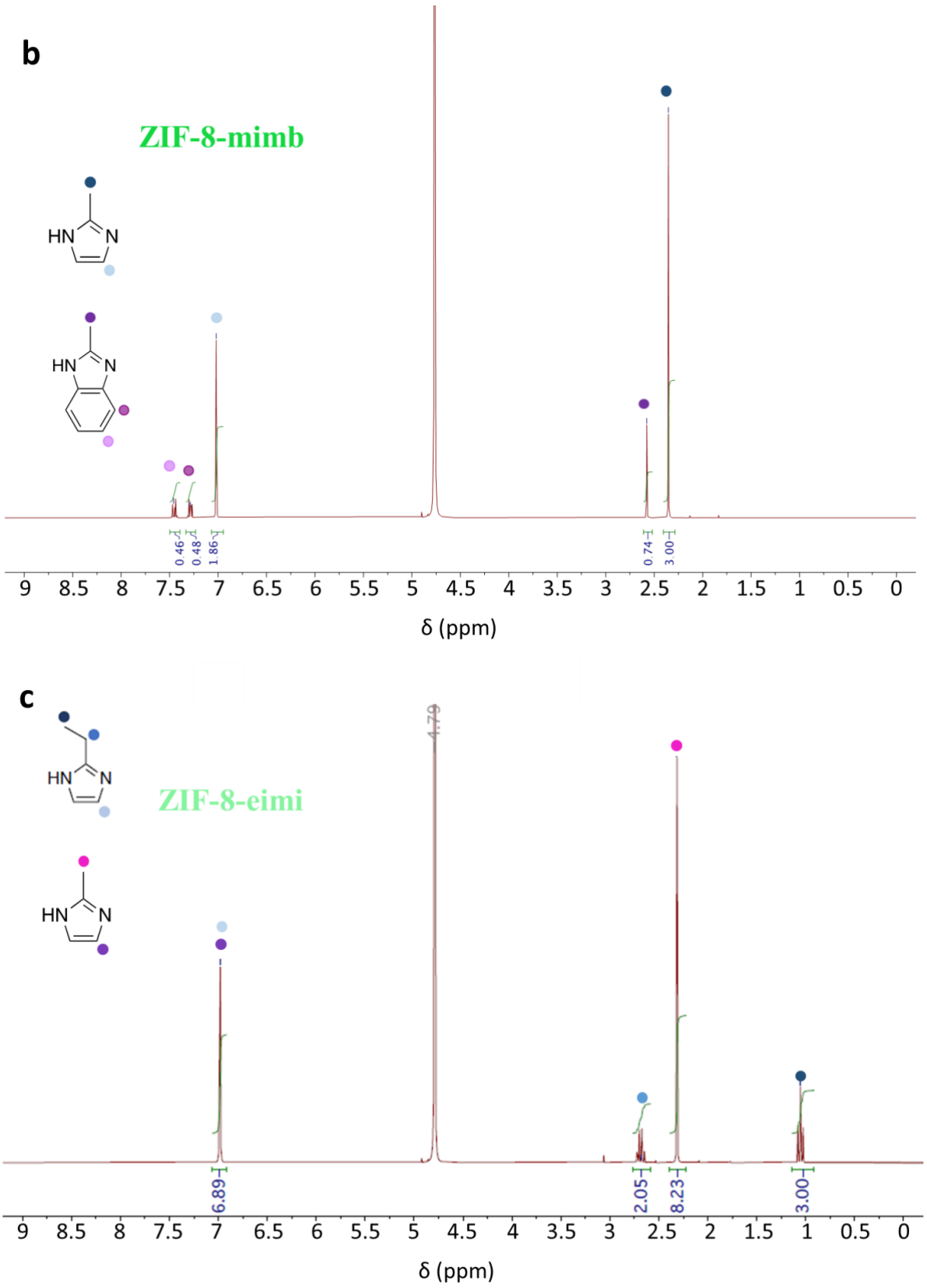

Figure S9. ^{1}H NMR spectra of digested **ZIF-8-eimb**, **ZIF-8-mimb** and **ZIF-8-eimi**. Coloured circles help to localize the corresponding chemical shifts of the protons.

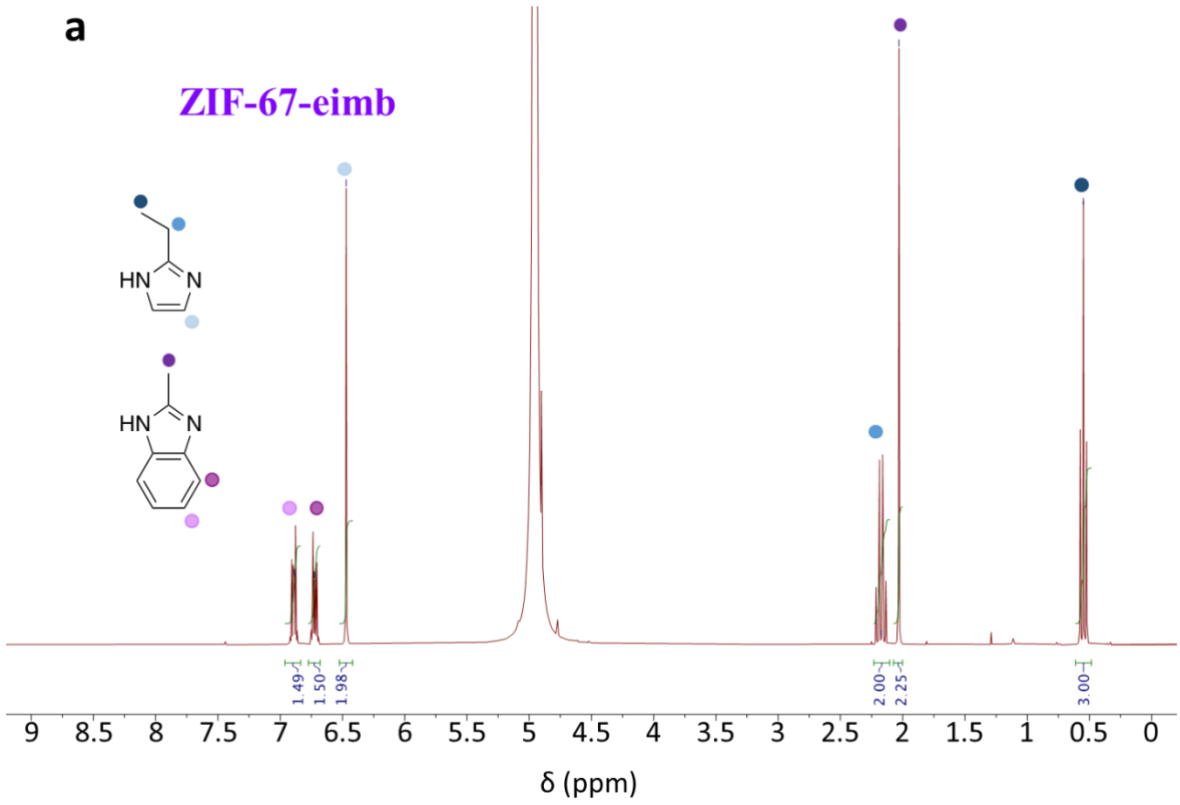
a
ZIF-67-eimb
HN
N
HN
N
1.49
1.50
1.98
2.00
2.25
3.00
9 8.5 8 7.5 7 6.5 6 5.5 5 4.5 4 3.5 3 2.5 2 1.5 1 0.5 0
δ (ppm)

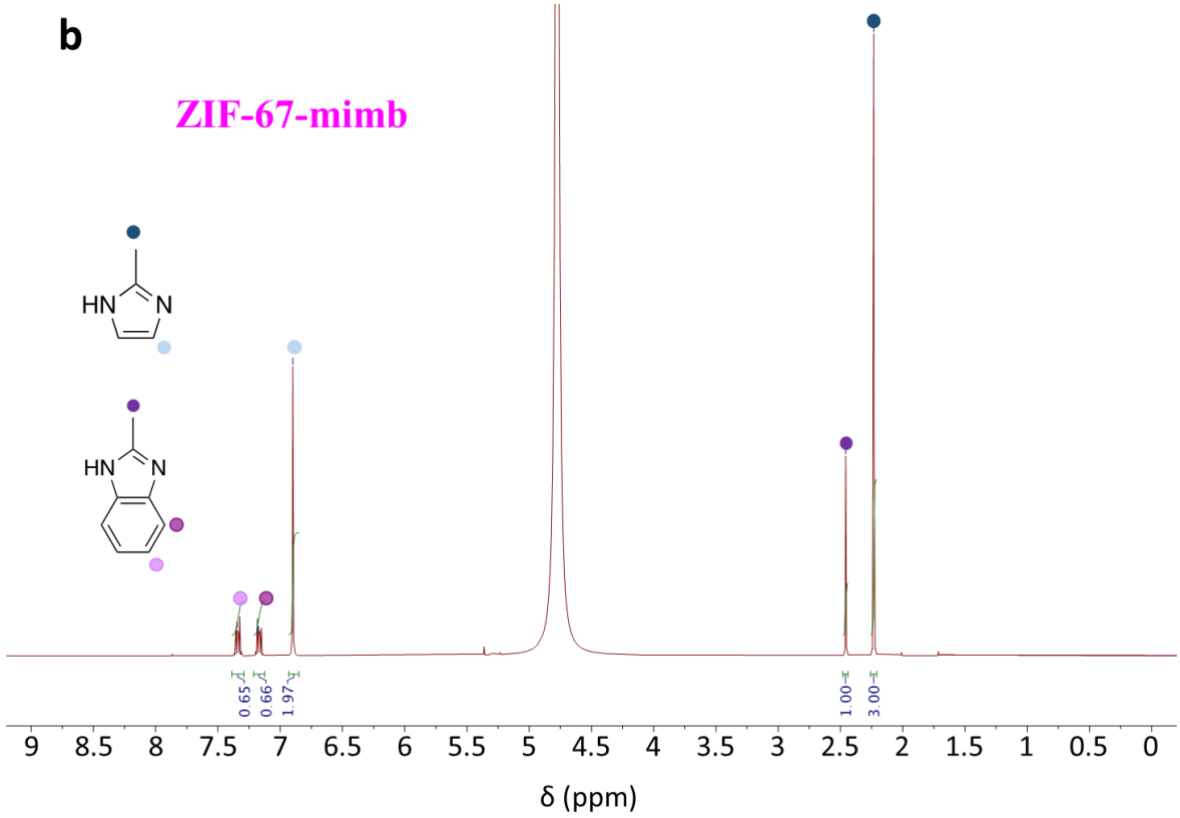
b
ZIF-67-mimb
HN
N
HN
N
0.65
0.66
1.97
1.00
3.00
9 8.5 8 7.5 7 6.5 6 5.5 5 4.5 4 3.5 3 2.5 2 1.5 1 0.5 0
δ (ppm)

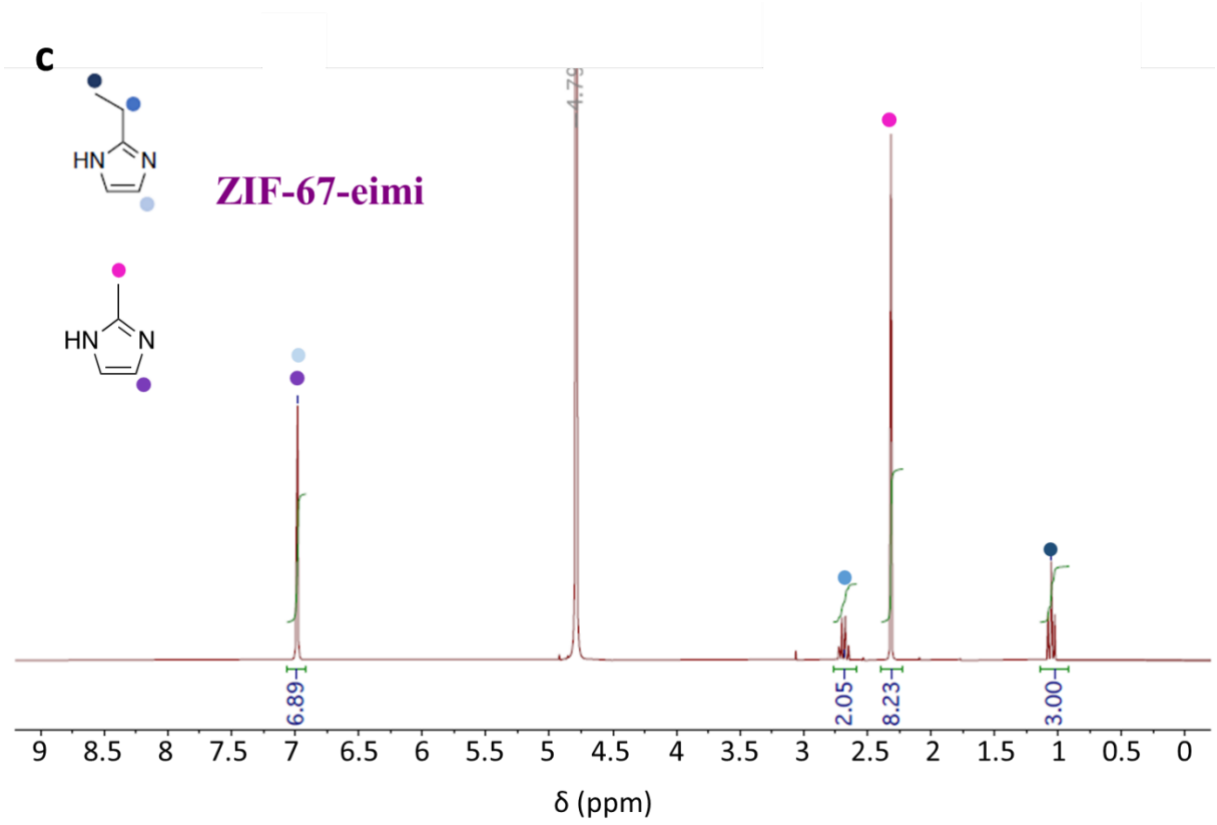

Figure S10. ^{1}H NMR spectra of digested **ZIF-67- eimb**, **ZIF-67-mimb** and **ZIF-67-eimi.** Coloured circles help to localize the corresponding chemical shifts of the protons.

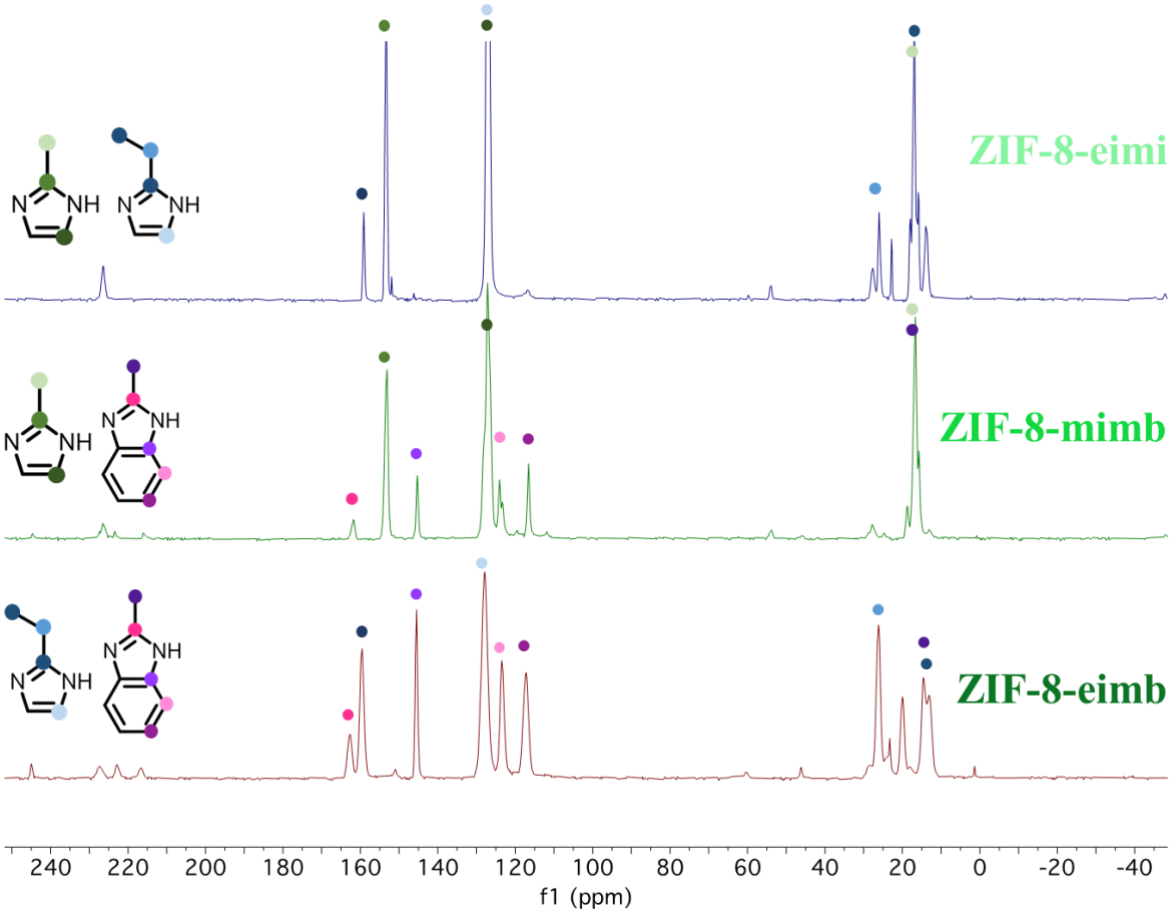

Figure S11. Solid state ^{13}C NMR spectra of **ZIF-8-eimb**, **ZIF-8-mimb** and **ZIF-8-eimi**. Coloured circles help to localize the corresponding chemical shifts of the protons.

The incorporated linker ratio output was obtained by NMR ^{1}H spectroscopy of digested samples and compared with the synthetic input. As shown in Table S3, the structurally incorporated output is normally close to the synthetic input, although the inclusion of the bulkier 2-methylbenzimidazole is limited to 40%, in agreement with the theoretical calculations (see main text).

Table S3. Comparison between the structurally incorporated output and synthetic input of the linker ratios for different samples with varied linker combinations in **MUV-3-eimb**, **MUV-3-mimb**, **ZIF-8-eimb**, **ZIF-8-mimb**, **ZIF-8-miei**, **ZIF-67-eimb, ZIF-67-mimb** and **ZIF-67-miei**.

MOF	Linker ratio	metal	synthetic input	structurally incorporated output
MUV-3-eimb	ei:mb	Fe(II)	50-50	62-38
MUV-3-eimb	ei:mb	Fe(II)	66-34	65-35
MUV-3-eimb	ei:mb	Fe(II)	66-34	67-33
MUV-3-eimb	ei:mb	Fe(II)	70-30	70-30
MUV-3-eimb	ei:mb	Fe(II)	75-25	70-30
MUV-3-mimb	mi:mb	Fe(II)	75-25	80-20
MUV-3-mimb	mi:mb	Fe(II)	65-35	66-34
ZIF-8-eimb	ei:mb	Zn(II)	50-50	57-43
ZIF-8-eimb	ei:mb	Zn(II)	50-50	60-40
ZIF-8-eimb	ei:mb	Zn(II)	66-34	70-30
ZIF-8-eimb	ei:mb	Zn(II)	66-34	70-30
ZIF-8-mimb	mi:mb	Zn(II)	66-34	80-20
ZIF-8-mimb	mi:mb	Zn(II)	66-34	79-21
ZIF-8-miei	mi:ei	Zn(II)	66-34	67-33
ZIF-67-eimb	ei:mb	Co(II)	50-50	57-43
ZIF-67-eimb	ei:mb	Co(II)	66-34	74-26
ZIF-67-eimb	ei:mb	Co(II)	66-34	69-31
ZIF-67-mimb	mi:mb	Co(II)	66-34	79-21
ZIF-67-miei	mi:ei	Co(II)	66-34	73-27

S2.5 Thermal stability

Thermogravimetric analysis of **MUV-3-eimb**, **MUV-3-mimb, ZIF-8- eimb**, **ZIF-8- mimb, ZIF-8-eimi, ZIF-67- eimb**, **ZIF-67- mimb, ZIF-67-eimi, MUV-6** and **MUV-7** were carried out with a TA instruments TGA 550 apparatus in the 25–650 °C temperature range under a 20°C·min^{-1} scan rate and a N_2 flow of 40 mL·min^{-1} for Fe(II) materials and air flow 40 mL·min^{-1} for the rest of materials. The thermogravimetric analyses show two similar plots for the **ZIF-8-mimb** and **ZIF-8-eimi** materials, losing around the 10% of mass at low temperatures (150°) (see Figure S13). This mass loss is likely caused by the presence of solvent molecules in the pores from the washing procedure (note that the two compounds that present a large mass loss, i.e. ZIF-8-eimi and ZIF-8-mimb, are the most porous ones according to the N_2 sorption isotherms, see Figure 3). After an activation at 150° under vacuum, this mass loss disappears almost completely in the TGA (see Figure S14).

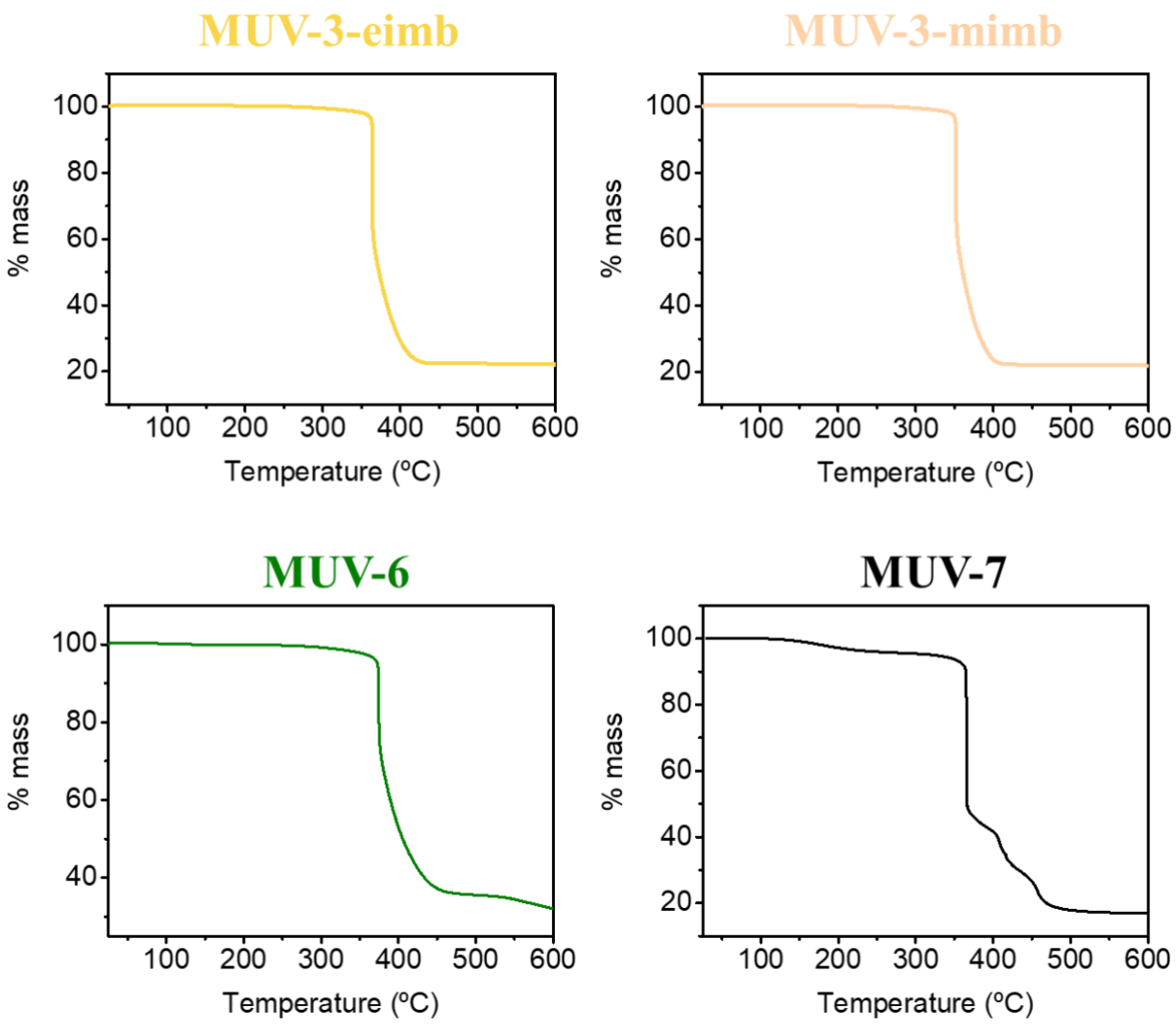

Figure S12. Thermogravimetric analysis of synthesized **MUV-6**, **MUV-7, MUV-3-mimb** and **MUV-3-eimb** in nitrogen gas at a heating rate of 20 ºC min^{-1}.

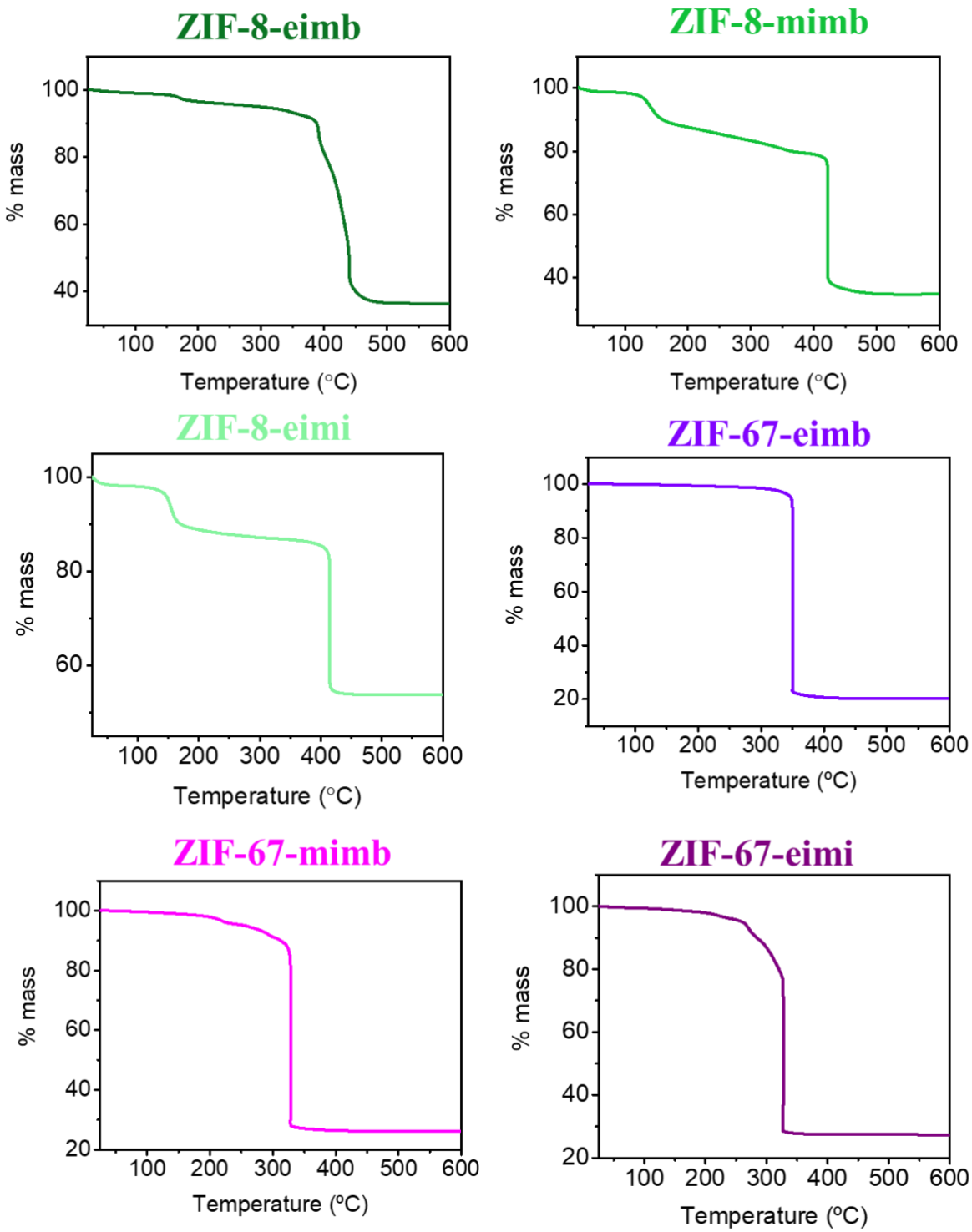

Figure S13. Thermogravimetric analysis of the as synthesized mixed-ligand derivatives of Zn(II) and Co(II).

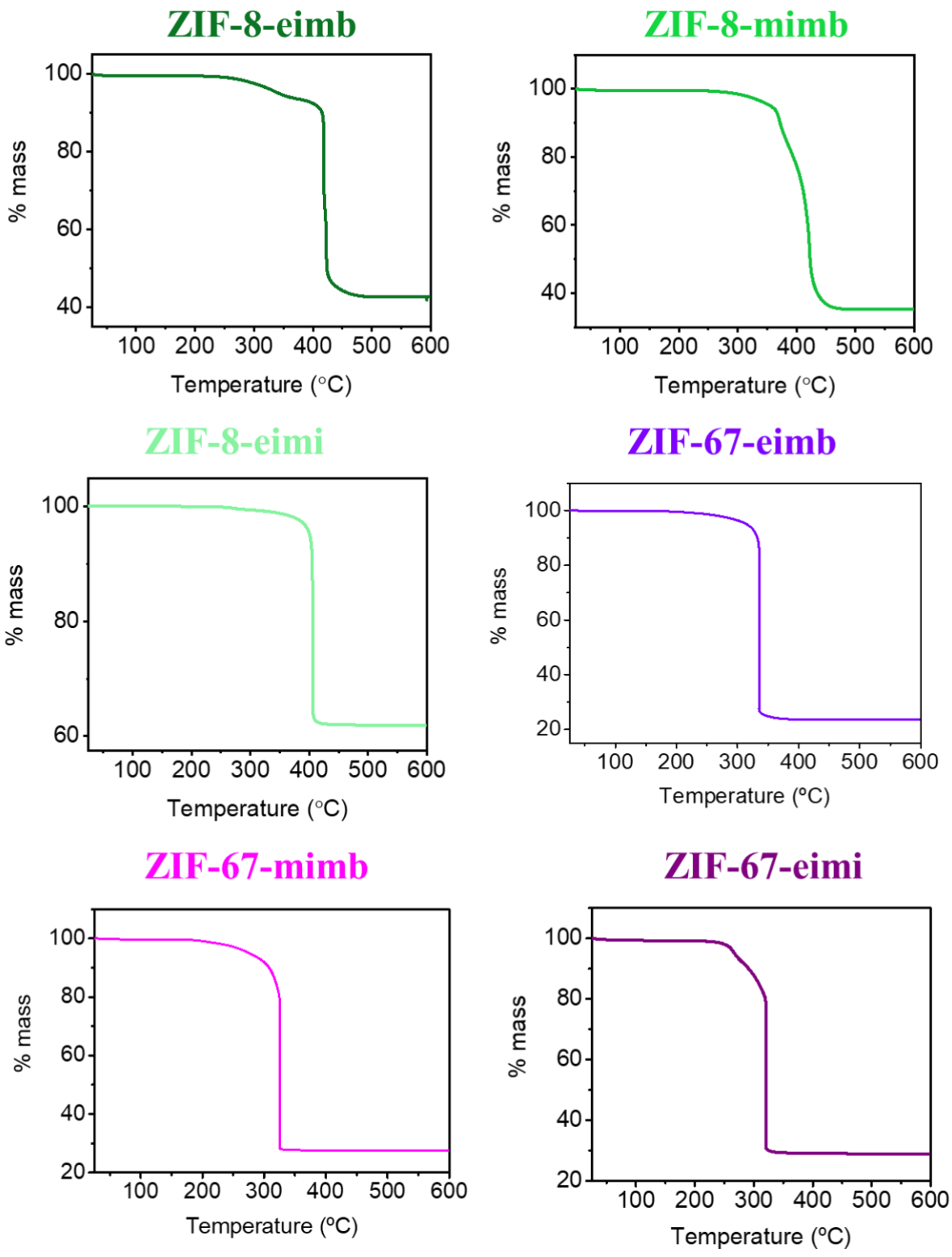

Figure S14. Thermogravimetric analysis of the activated mixed-ligand derivatives of Zn(II) and Co(II).

S2.6 Infrared spectroscopy

IR were recorded in a Platinum-ATR diamond Bruker spectrometer in the 4000−400 cm^{-1} range using powdered samples. The different functional groups are clearly detected by the presence of different peaks in the IR spectra. These differences can also be appreciated also in the mixed-ligand ZIFs, thus confirming the presence of two different ligands.

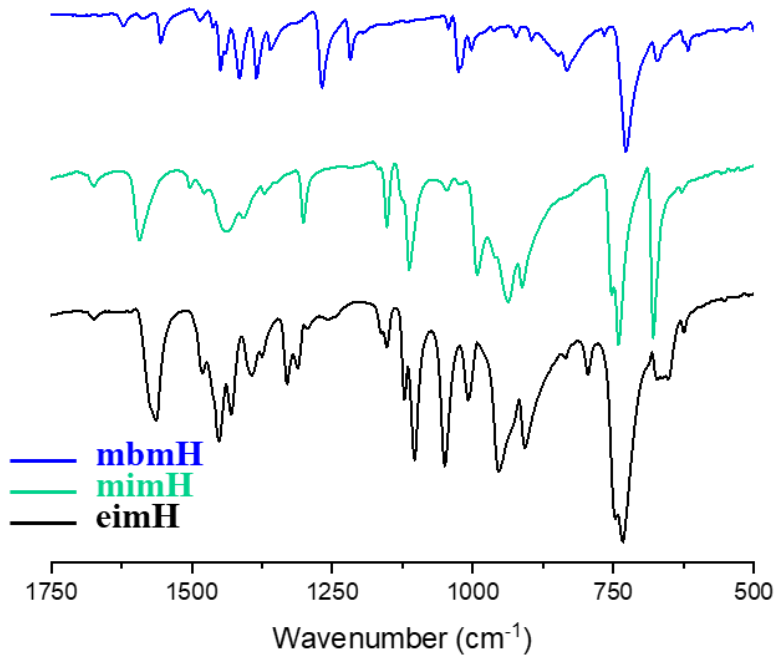

Figure S15. Infrared spectra of ligands 2-methylbenzimidazole (mbH), 2-methylimidazole (miH) and 2-ethylimidazole (eiH).

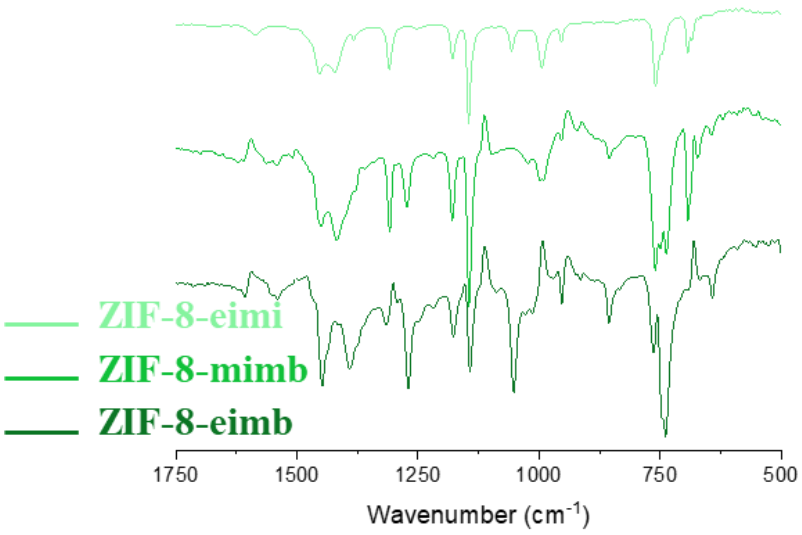

Figure S16. Infrared spectra of **ZIF-8-eimi**, **ZIF-8-mimb** and **ZIF-8-eimb**.

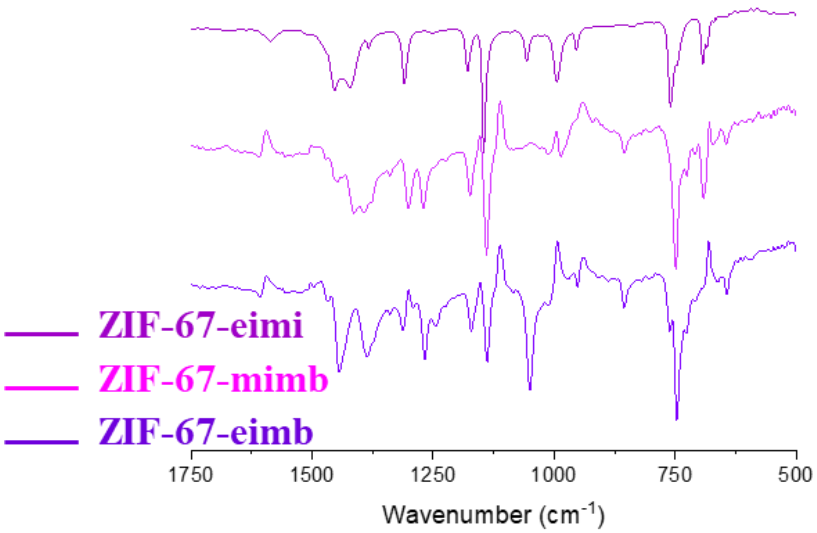

Figure S17. Infrared spectra of **ZIF-67-eimi**, **ZIF-67-mimb** and **ZIF-67-eimb**.

S2.7 Scanning electron microscopy

Scanning Electronic Micrographs images were recorded in a Hitachi S-4800.

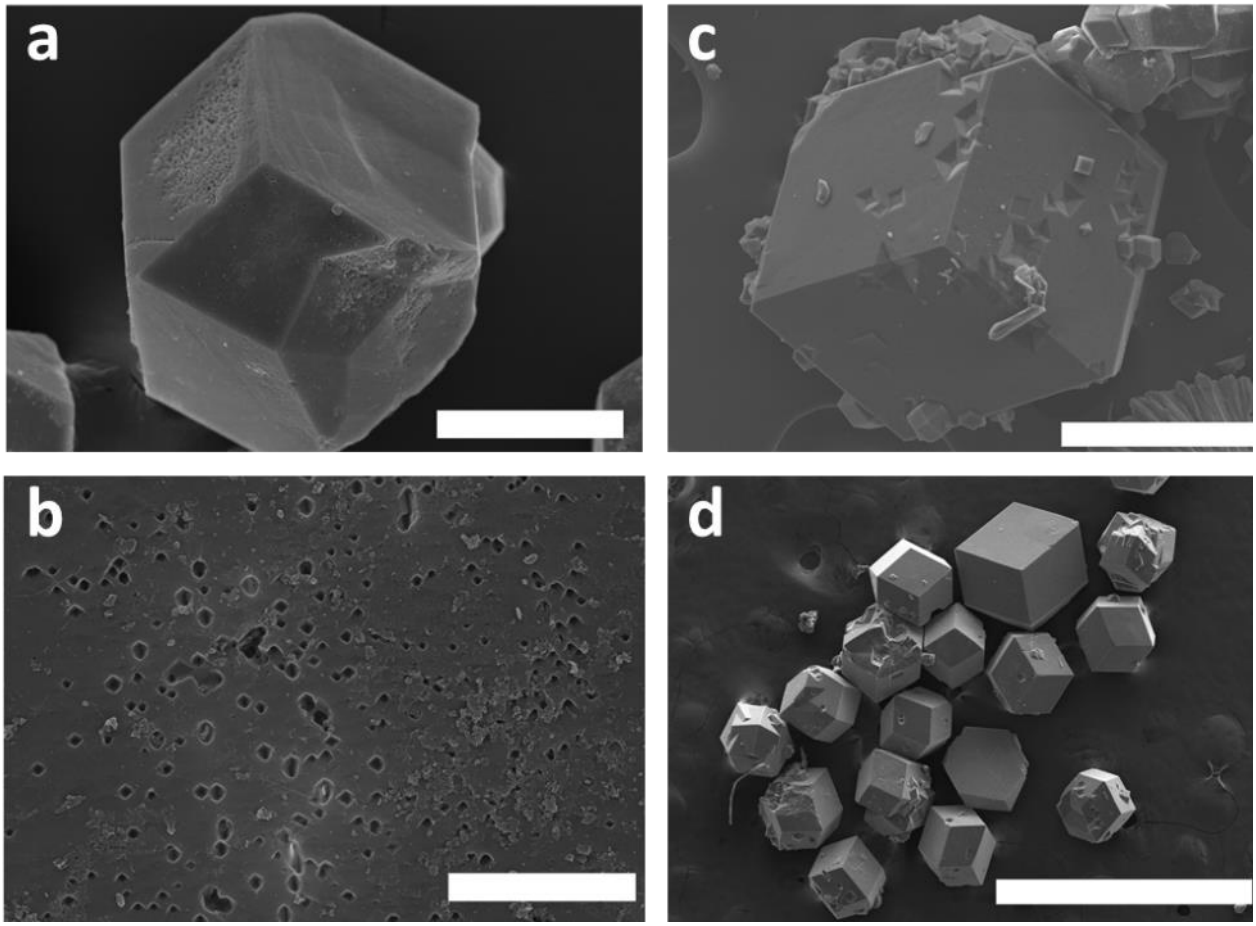

Figure S18. a) A single crystal of **MUV-3-mimb** with rhombohedral morphology. Scale bar 50 μm b) Zoom of the surface of the crystal (a), with rhombohedral holes. Scale bar 5 μm c) A single-crystal of **MUV-3-eimb**. Scale bar 200 μm. d) A representative sample of **MUV-3-eimb** crystals. Scale bar 1 mm.

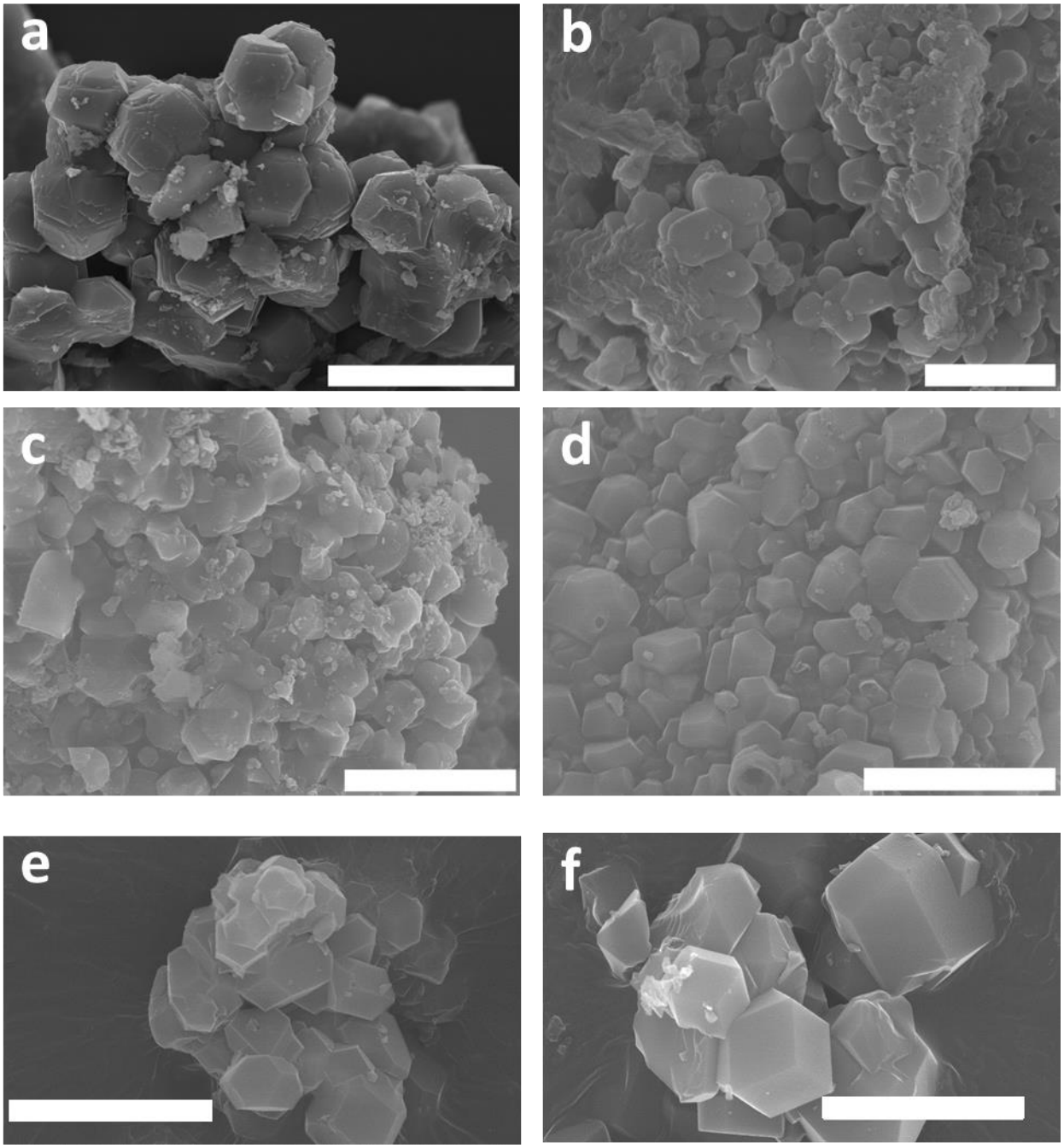

Figure S19. a) Crystals of **ZIF-8-eimb** with defined morphology. Scale bar 20 μm. b) Crystals of **ZIF-8-mimb** with defined morphology, similar to ZIF-8. Scale bar 5 μm. c) Crystals of **ZIF-67-eimb**. Scale bar 20 μm. d) Crystals of **ZIF-67-mimb** with similar morphology to ZIF-67. Scale bar 10 μm. e) Crystals of **ZIF-8-eimi**. Scale bar 4 μm. f) Crystals of **ZIF-67-eimi** with similar morphology to ZIF-67. Scale bar 4 μm.

S2.8 N_2 and CO_2 gas sorption

Single-gas volumetric isotherms were carried out in a Tristar II Plus (Micromeritics), at 77 K and 298 K. N_2 sorption measurements were used to calculate BET values for **ZIF-8-mimb, ZIF-8-eimi** and **ZIF-67-eimi**, showing BET values of 875, 845, and 402 m^2/g, respectively. For the other compounds, CO_2 isotherms were used to calculate an approximate value of BET surface, with values of ca. 80 m^2/g for each compound.

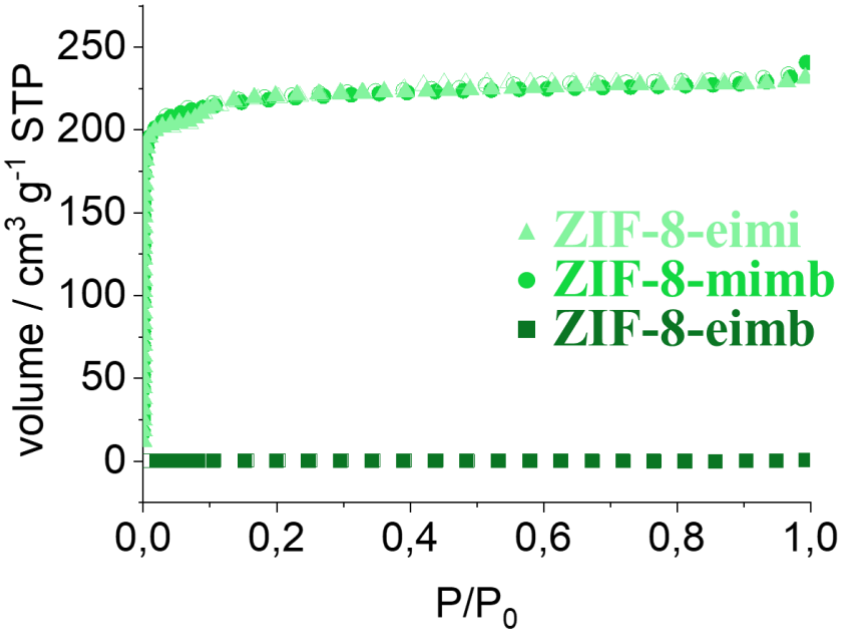

Figure S20. N_2 sorption (solid figures) and desorption (open figures) of **ZIF-8** mix-ligand materials at 77 K.

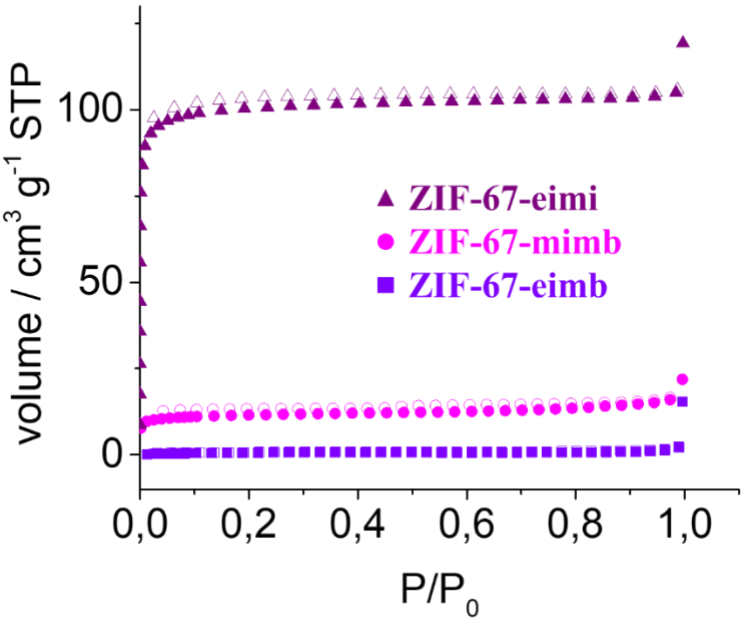

Figure S21. N_2 sorption (solid figures) and desorption (open figures) of **ZIF-67** mix-ligand materials at 77 K.

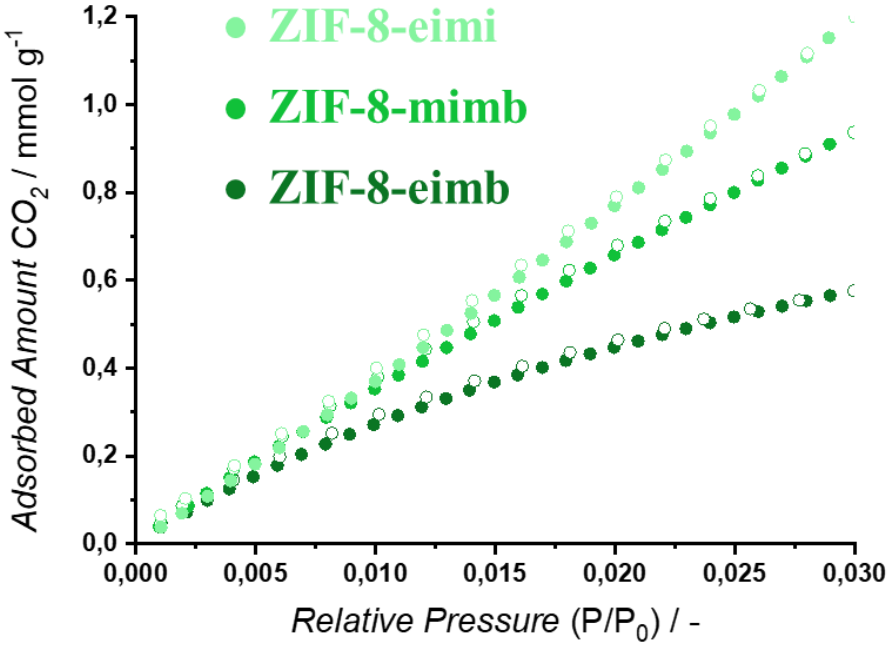

Figure S22. CO_2 sorption (solid figures) and desorption (open figures) of **ZIF-8** mix-ligand materials at 298 K.

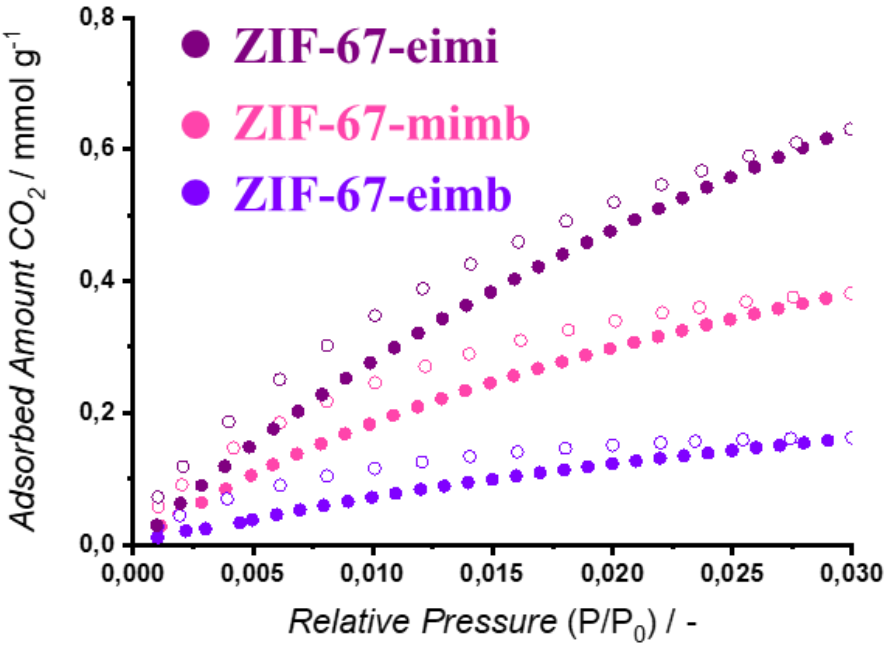

Figure S23. CO_2 sorption (solid figures) and desorption (open figures) of **ZIF-67** mix-ligand materials at 298 K.

S3 Theoretical calculations

Theoretical calculations were performed under the Density Functional Theory (DFT) framework by using the all-electron full-potential FHI-AIMS electronic structure code package.[5] Initial ZIF geometries were extracted from available experimental CIF data. Minimum-energy crystal structures were obtained after full lattice and ion relaxation through the GGA-type PBEsol functional[6] and the numeric atom-centered orbital (NAO) tier-1 basis set.[7] No symmetry constraints were applied along the geometry optimization. Dispersion forces were assessed by means of the vdW correction based on Hirshfeld partitioning of the electron density as described by Tkatchenko and Scheffler.[8] However, we found that this correction overestimates weak noncovalent forces, especially when modelling 2mbim-based ZIFs, thus providing a wrong picture of phase stability even between pure-ligand materials (see Table S4). We therefore switched off the dispersion correction for the data shown in the main text. Relative phase stability was calculated from absolute energies considering all the ligands involved in the ZIF material for a particular metal atom:

$$\text{pure-ligand MOFs: } MX_2 + Y_2 + Z_2 \quad \leftrightarrow \quad MY_2 + X_2 + Z_2 \quad \leftrightarrow \quad MZ_2 + X_2 + Y_2$$

$$\text{mixed-ligand MOFs: } \quad MY_{2(1-a)}Z_{2a} + X_2 + Y_{2a} + Z_{2(1-a)}$$

where M = Zn, Co or Fe; X, Y, Z = 2mim, 2eim and 2mbim, respectively; and a = 2mbim fraction in a 2eim–2mbim mixing.

Both Co- and Fe-based MOFs were considered in their high-spin configuration. Thus, the initial spin moment was set to 3 and 4 for Co(II) and Fe(II) atoms, respectively. Ligand substitution was modelled from the pure-ligand optimized crystal structure closer to the target composition by using the Chemcraft 1.8 software.[9] Crystal structures were visualized and analysed through the VESTA program.[10]

Table S4. Cell parameters calculated for the minimum-energy crystal structures of zeolitic MOFs as a function of the topology (*dia*, *qtz* or SOD), metal atom (Zn, Fe or Co), ligand (2mim, 2eim or 2mbim) and 2eim:2mbim ratio (2mbim fraction) at the PBEsol level of theory.

System	E_{rel} (eV)	*a* (Å)	*b* (Å)	*c* (Å)	α (°)	β (°)	γ (°)	V (Å^3)	ρ (g/cm^3)
				Zn					
mim-*dia*	0.030	7.954	8.186	16.974	89.8	89.9	90.6	1105.2	1.368
eim-*dia*	0.262	8.652	8.841	16.456	89.9	90.3	90.5	1258.6	1.349
mbim-*dia*	0.246	8.877	9.179	16.226	90.0	89.9	90.0	1322.2	1.646
eimb-0.25-*dia*	0.260	8.971	8.556	16.613	89.6	90.6	89.0	1274.8	1.426
eimb-0.50-*dia*	0.282	8.787	8.946	16.414	89.2	89.7	88.7	1289.8	1.502
eimb-0.75-*dia*	0.269	8.980	8.915	16.393	88.5	90.0	90.3	1312.0	1.568
mim-*qtz*	0.047	8.477	8.464	12.775	90.0	90.1	120.5	789.4	1.436
eim-*qtz*	0.121	8.475	8.470	12.694	89.9	90.1	119.5	793.2	1.605
mbim-*qtz*	1.164	9.309	9.750	13.215	81.7	94.1	102.1	1159.3	1.408
eimb-0.33-*qtz*	0.608	8.935	9.258	13.026	82.3	87.5	104.7	1029.5	1.353
eimb-0.66-*qtz*	1.038	9.156	9.299	13.473	81.4	93.3	103.8	1101.0	1.374
mim-SOD	0.000	16.874	16.873	16.849	90.0	90.0	90.0	4797.0	0.945
eim-SOD	0.202	17.193	17.068	17.139	89.1	91.3	89.4	5027.1	1.013
mbim-SOD	0.293	17.136	17.151	17.086	90.0	89.9	90.1	5021.7	1.300
eimb-0.33-SOD	0.127	17.068	16.964	16.974	90.1	90.9	91.1	4913.2	1.134
eimb-0.67-SOD	0.252	16.898	16.923	16.974	82.1	91.3	87.6	5025.8	1.204
				Co					
mim-*dia*	0.025	7.875	8.115	16.963	89.9	89.9	90.4	1083.9	1.355
eim-*dia*	0.270	8.614	8.719	16.448	89.9	90.3	90.7	1235.3	1.340
mbim-*dia*	0.254	8.847	9.139	16.188	90.0	89.9	90.0	1308.9	1.630
eimb-0.25-*dia*	0.269	8.932	8.529	16.581	89.6	90.6	88.9	1262.8	1.405
eimb-0.50-*dia*	0.293	8.746	8.832	16.436	89.0	89.5	88.4	1269.0	1.493
eimb-0.75-*dia*	0.277	8.932	8.529	16.581	89.6	90.6	88.9	1262.8	1.595
mim-*qtz*	0.017	8.368	8.317	12.798	90.0	90.1	120.9	763.9	1.442
eim-*qtz*	0.107	8.442	8.440	12.655	89.8	90.2	119.7	783.3	1.585
mbim-*qtz*	1.243	9.364	9.693	12.963	82.5	95.0	103.2	1133.8	1.411
eimb-0.33-*qtz*	0.699	8.973	9.107	12.984	81.1	87.0	104.0	1012.9	1.344
eimb-0.66-*qtz*	1.135	9.338	9.067	9.067	80.0	92.9	102.0	1088.3	1.361
mim-SOD	0.000	16.794	16.798	16.771	90.0	90.0	90.0	4731.1	0.931
eim-SOD	0.209	17.137	17.012	17.081	89.1	91.4	89.4	4977.5	0.998
mbim-SOD	0.277	17.064	17.079	17.014	90.0	89.9	90.1	4958.5	1.291
eimb-0.33-SOD	0.119	16.899	16.985	16.710	88.0	91.8	92.9	4785.2	1.138
eimb-0.67-SOD	0.261	16.731	16.825	17.168	84.2	90.2	87.3	4931.3	1.201
				Fe					
mim-*dia*	0.076	7.882	8.152	17.268	89.9	90.0	90.3	1109.5	1.305
eim-*dia*	0.188	8.700	8.700	16.735	89.8	90.1	91.9	1267.0	1.290
mbim-*dia*	0.097	8.902	9.199	16.315	90.0	90.0	90.0	1336.0	1.582
eimb-0.25-*dia*	0.164	9.019	8.534	16.793	89.7	90.9	88.3	1291.8	1.358
eimb-0.50-*dia*	0.171	8.814	8.969	16.486	89.3	89.7	88.9	1302.8	1.438
eimb-0.75-*dia*	0.137	8.987	8.908	16.537	88.3	89.8	90.4	1323.3	1.507

mim-*qtz*	0.062	8.483	8.470	12.904	90.0	90.1	120.4	799.9	1.358
eim-*qtz*	0.113	8.505	8.497	12.779	89.9	90.1	119.8	801.6	1.529
mbim-*qtz*	1.252	9.348	9.725	13.209	81.9	94.7	102.4	1159.6	1.367
eimb-0.33-*qtz*	0.666	9.091	9.091	13.138	82.2	87.6	104.1	1040.2	1.294
eimb-0.66-*qtz*	1.161	9.237	9.319	13.460	80.6	92.7	103.5	1111.5	1.318
mim-SOD	0.000	16.933	16.937	16.978	89.9	90.0	90.0	4869.2	0.892
eim-SOD	0.167	17.288	17.161	17.224	89.0	91.5	89.4	5107.2	0.960
mbim-SOD	0.158	17.173	17.188	17.123	90.0	89.9	90.1	5054.1	1.254
eimb-0.33-SOD	0.111	17.166	17.061	17.066	89.6	91.3	91.2	4995.5	1.077
eimb-0.67-SOD	0.135	16.894	16.990	17.283	83.0	90.6	87.0	5080.4	1.154

Table S5. Cell parameters calculated for the experimentally resolved crystal structures of various ZIFs.

	a (Å)	*b* (Å)	*c* (Å)	*α* (°)	*β* (°)	*γ* (°)	V (Å^3)	*ρ* (g/cm^3)
ZIF-8 (mim-SOD)	16.993	16.993	16.993	90.0	90.0	90.0	4906.9	0.924
MUV-3 (eimb-SOD)	17.300	17.300	17.300	90.0	90.0	90.0	5177.5	1.040
MUV-7 (mbim-*dia*)	9.243	9.350	15.988	90.0	90.0	90.0	1381.8	1.529
MUV-6 (eim-*qtz*)	8.421	8.421	13.170	90.0	90.0	120.0	808.7	1.516

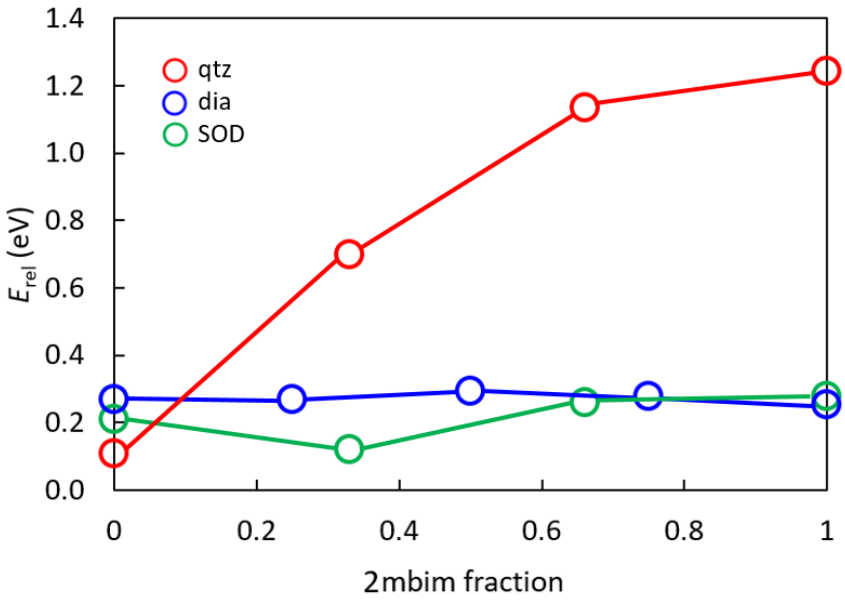

Figure S24. Phase stability diagram calculated at the PBEsol level for mixed 2eim:2mbim Co-based ZIF-67 with respect to the most stable pure-2mim ZIF. Lines are drawn to guide the eye.

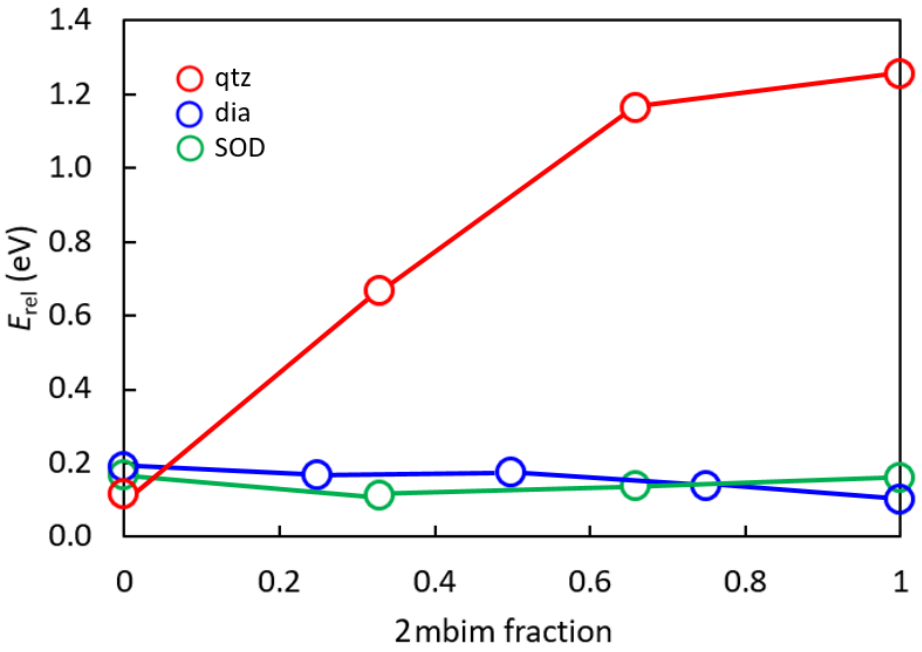

Figure S25. Phase stability diagram calculated at the PBEsol level for mixed 2eim:2mbim Fe-based **MUV-3** with respect to the most stable pure-2mim ZIF. Lines are drawn to guide the eye.

Table S6. Relative energy calculated for the minimum-energy crystal structures of Zn-based ZIF-8 ZIFs as a function of the topology (*dia*, *qtz* or SOD), ligand (2mim, 2eim or 2mbim) and 2eim:2mbim ratio (2mbim fraction) at the PBEsol level of theory including vdW dispersion corrections.

System	E_{rel} (eV)
mim-*dia*	0.327
eim-*dia*	0.383
mbim-*dia*	0.000
eimb-0.25-*dia*	0.430
eimb-0.50-*dia*	0.331
eimb-0.75-*dia*	0.169
mim-*qtz*	0.623
eim-*qtz*	0.185
mbim-*qtz*	0.965
eimb-0.33-*qtz*	0.788
eimb-0.66-*qtz*	1.016
mim-SOD	0.647
eim-SOD	0.662
mbim-SOD	0.645
eimb-0.33-SOD	0.445
eimb-0.66-SOD	0.454

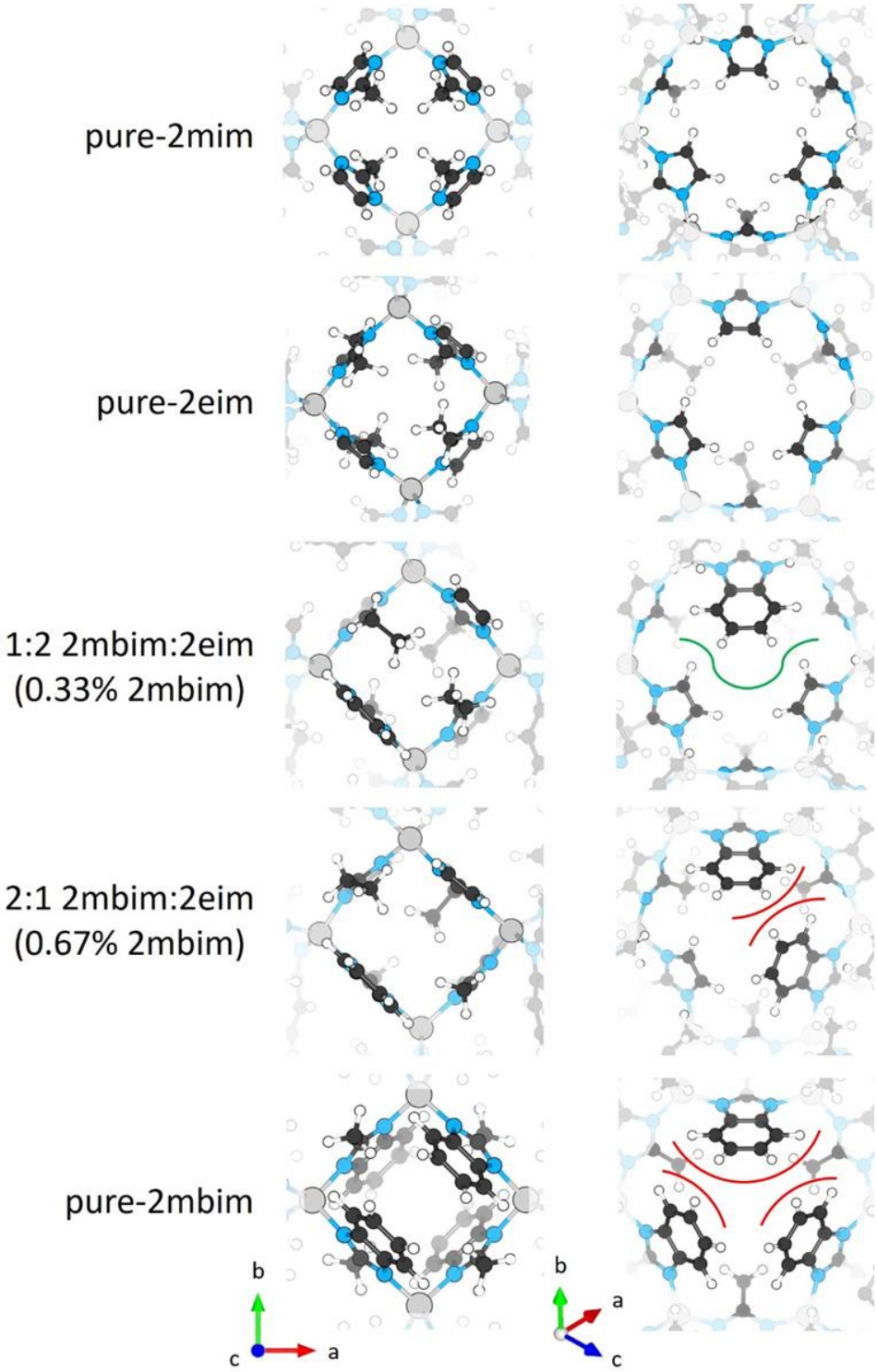

Figure S26. Axis (left) and diagonal (right) views of the minimum-energy crystal structure calculated for Zn-based ZIF-8 ZIFs as a function of ligand composition at the PBEsol level.

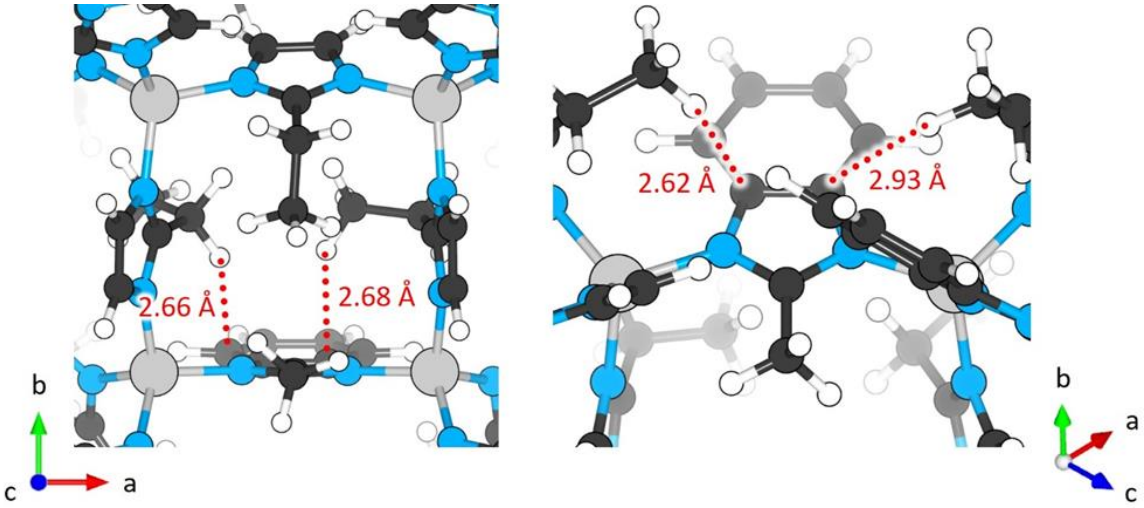

Figure S27. Minimum-energy crystal structure of mixed-ligand ZIF-8 with 1:2 2mbim:2eim ratio (0.33% 2mbim) displaying relevant short CH···π interactions between the ethyl group of the eim ligand and the benzene imidazole π -system of the mbim ligand.

S4 Water stability characterization

Crystals of **MUV-3-eimb** and **MUV-3-mimb** were exposed to air in ambient conditions during 24 hours and 48 hours (Figure S28). 12 mg of several materials (**ZIF-8-eimb**, **ZIF-8-mimb, ZIF-67-eimb**, **ZIF-67-mimb, ZIF-8** and **ZIF-67**) were immersed in 20 ml of water under permanent stirring for 48 hours. After this time, the water was evaporated in an oven at 40 °C. The obtained powder was checked by X-ray powder diffraction. For NMR studies, 1.2 mg of ZIFs were immersed in 2 ml of D_2O during 48 hours.

To check the instability of **ZIF-8** under the same condition, some samples of **ZIF-8** and **ZIF-67** were prepared by solvent-free conditions to compare the stabilities. Figure S29 shows the appearance of another unknown phase in the **ZIF-8** diffractogram,[11] which has been previously identified as $Zn(OH)(NO_3)(H_2O)$.[12] However, in this experiment there are no NO_3^- ions present, due to the solvent-free nature of the synthesis, using ZnO as a metallic source. **ZIF-67** seems to retain the crystal structure without the appearance of any additional phase (Figure S29). The four mixed-ligand structures present the same diffractogram as before the water treatment. The Zn(II) compounds seem more stable than the **ZIF-8**, and no extra peak is observed upon water treatment. However, X-ray diffraction does not reveal possible etching of the ligands caused by partial dissolution in water. Still, this can be detected by ^1H NMR spectroscopy. Thus, upon 48-hours immersion in D_2O, under continuous stirring, water samples were analyzed by H^1 NMR spectroscopy (Figures S30-S31). The comparison between ZIF-8/ZIF-67 and the mixed ligand ZIFs shows less etching of the material for the same time immersed in water. For a quantitative comparison, known volumes of the D_2O (from the ZIFs water immersed) were analyzed with an internal standard, $(CH_3)_4NCl$, with known concentration, as recent reported works.[13] The characteristics peaks from the different methyl groups were identify and the areas were normalized to quantify the linker ratios and concentration in the original water stability studies. For **ZIF-8** and **ZIF-67,** it was found a 48 % and 21 % of 2mimH in the D_2O, respective to the maximum possible molar ratio. For ZIF-eimb compounds, very similar percentages were found, 46 % for Zn(II) compound and 27 % for the Co(II) compound. However, for the ZIF-mimb series, lower percentages of ligands were found in the D_2O, 38 % for the Zn(II) material and 16% for the Co(II) material. Despite the major hydrophobicity and steric hindrance, the eimb mixtures present higher percentages of etching than the mimb series.

S4.1 X-ray powder diffraction

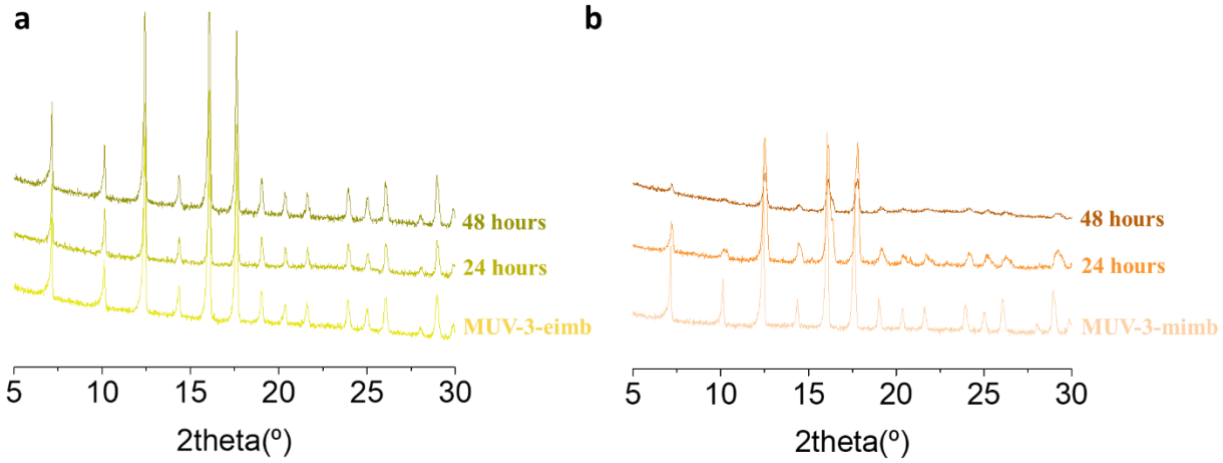

Figure S28. X-ray powder diffraction after 24 and 48 hours of exposition at air atmosphere for **MUV-3-eimb** and **MUV-3-mimb**.

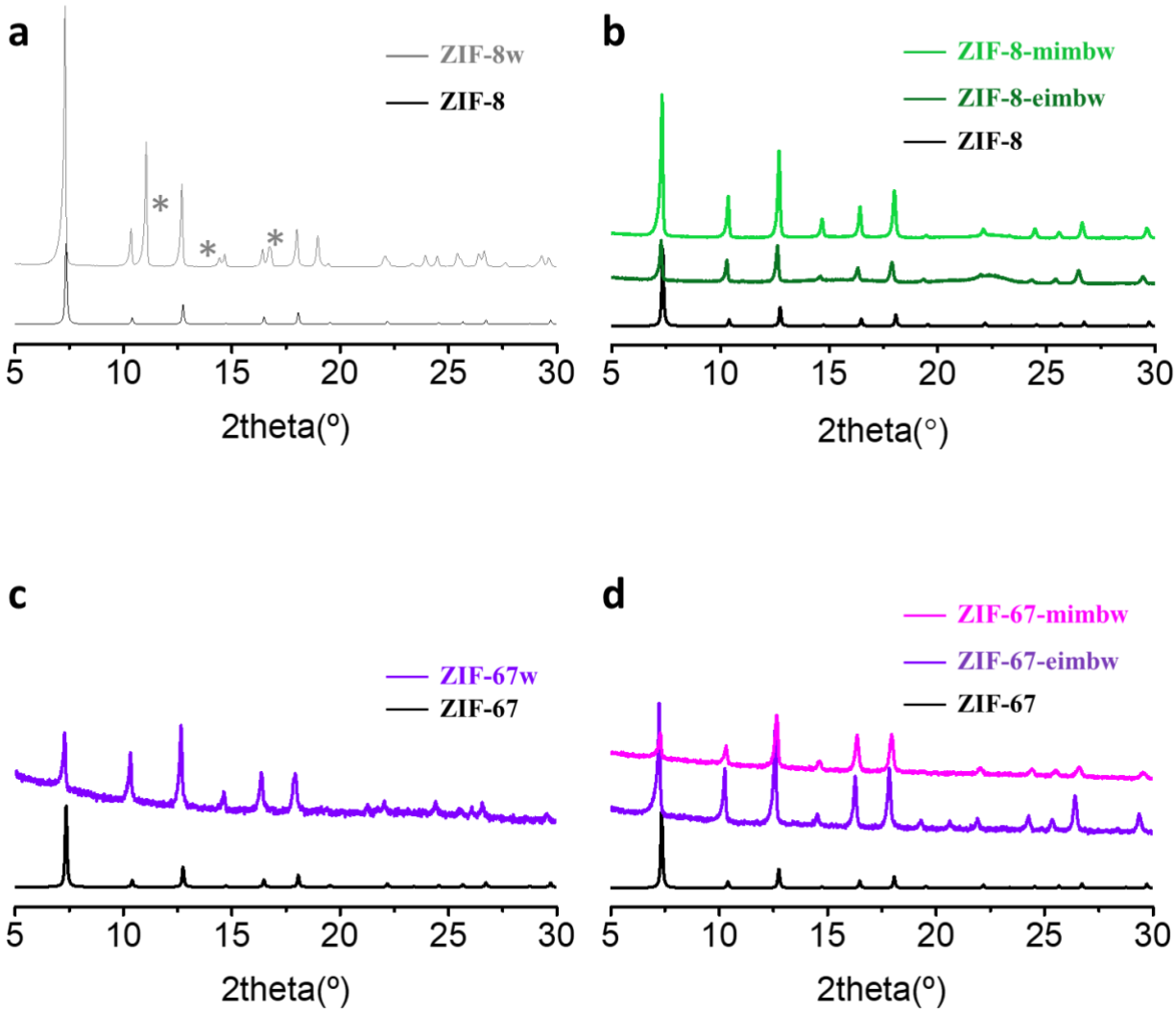

Figure S29. a) X-ray powder diffraction of ZIF-8 after 48 hours in water solution. The asterisk indicates the extra peaks of the unknown phase. b) X-ray powder diffraction of **ZIF-8-mimb** and **ZIF-8-eimb** after 48 hours in water solution. c) X-ray powder diffraction of **ZIF-67** after 48 hours in water solution. d) X-ray powder diffraction of **ZIF-67-mimb** and **ZIF-67-eimb,** after 48 hours in water solution.

S4.2 NMR spectroscopy

The etching ligand ratio was calculated with the following formula:

$$C_{lig} = \frac{\frac{I_{lig}}{3}}{\frac{I_p}{12}} * C_p$$

With the calculated concentration with a known volume, the moles of dissolved ligands were calculated and compared with the theoretical maximum moles achievable with a complete etching of ZIFs.

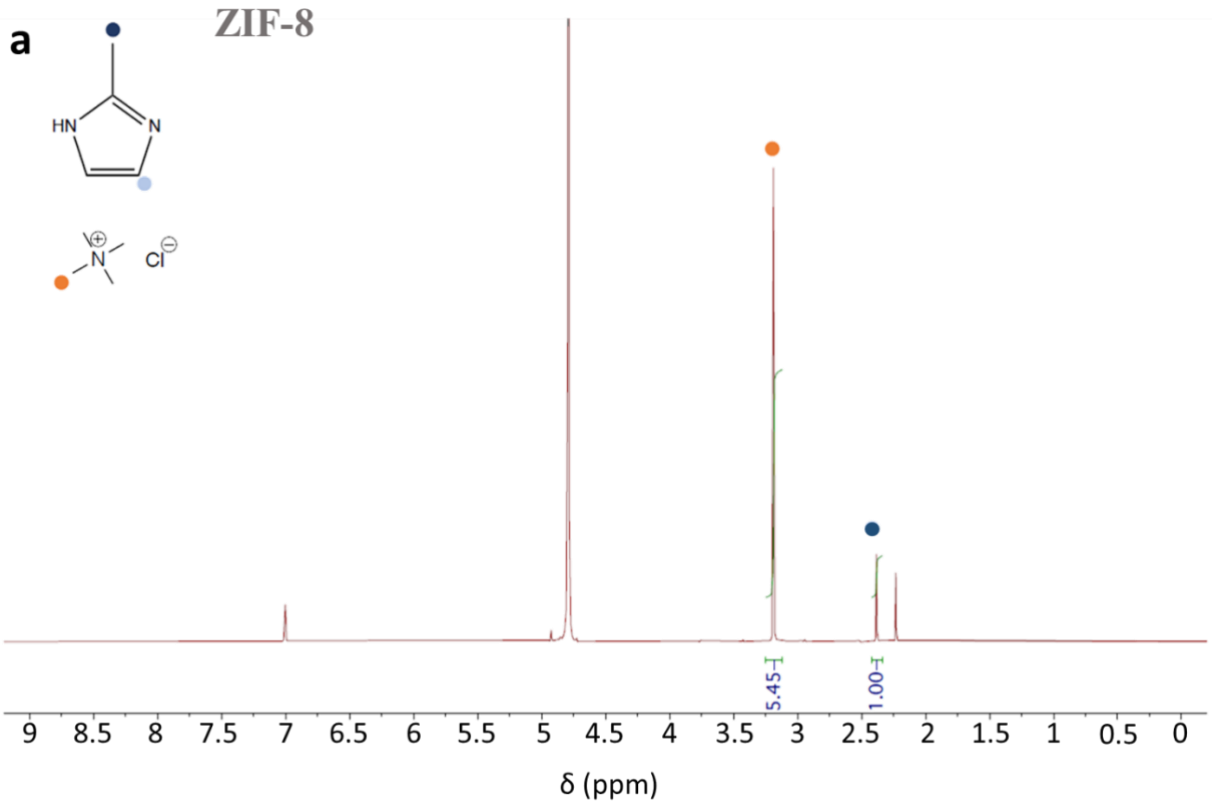
a
ZIF-8
HN
N
Cl
5.45
1.00
9 8.5 8 7.5 7 6.5 6 5.5 5 4.5 4 3.5 3 2.5 2 1.5 1 0.5 0
δ (ppm)

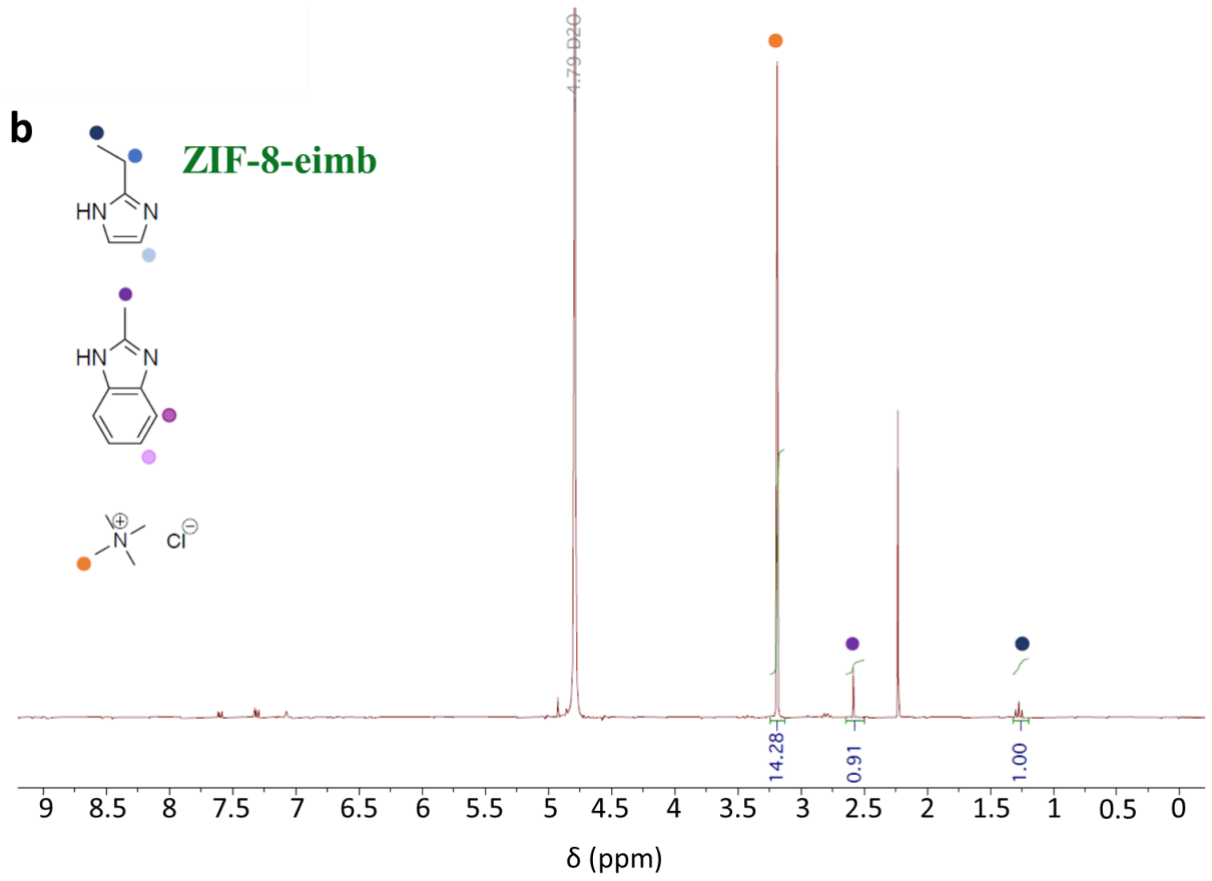
b
ZIF-8-eimb
HN
N
Cl
14.28
0.91
1.00
9 8.5 8 7.5 7 6.5 6 5.5 5 4.5 4 3.5 3 2.5 2 1.5 1 0.5 0
δ (ppm)

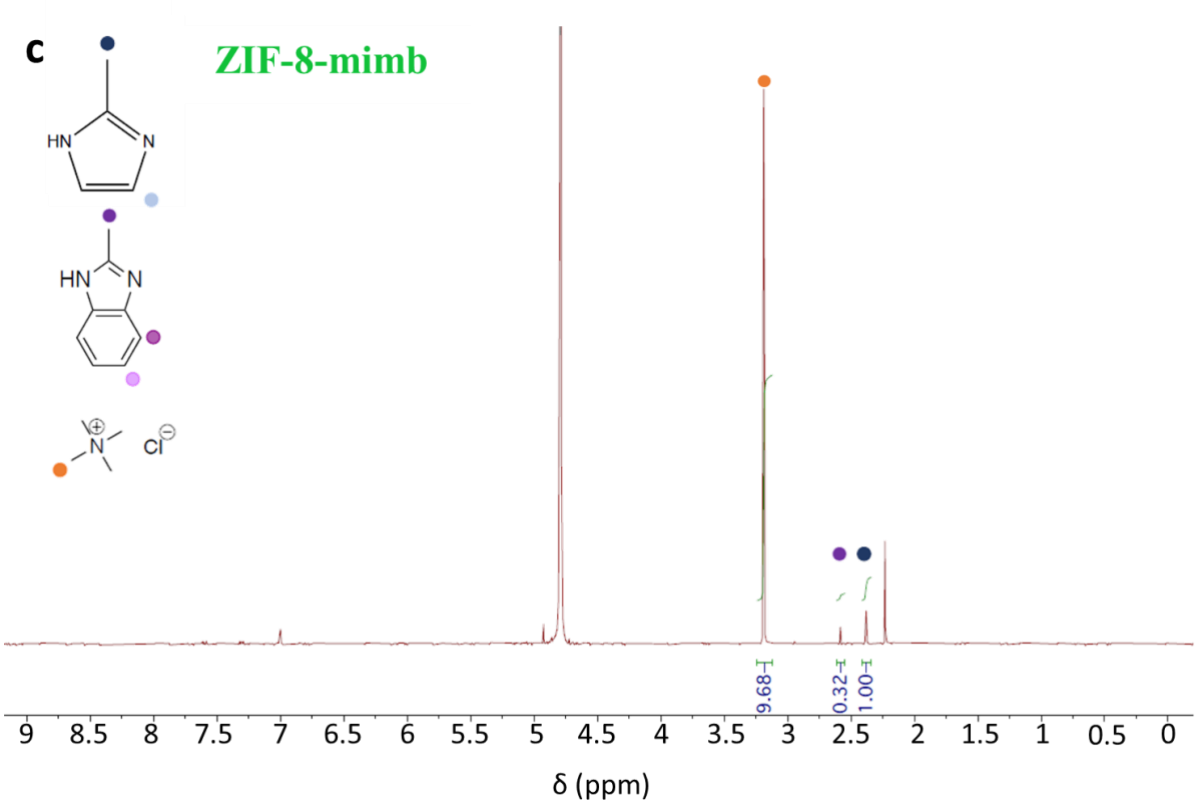

Figure S30. NMR spectra of **ZIF-8** (a), **ZIF-8-eimb** (b) and **ZIF-8-mimb** (c). Coloured circles help to localize the corresponding chemical shifts of the protons

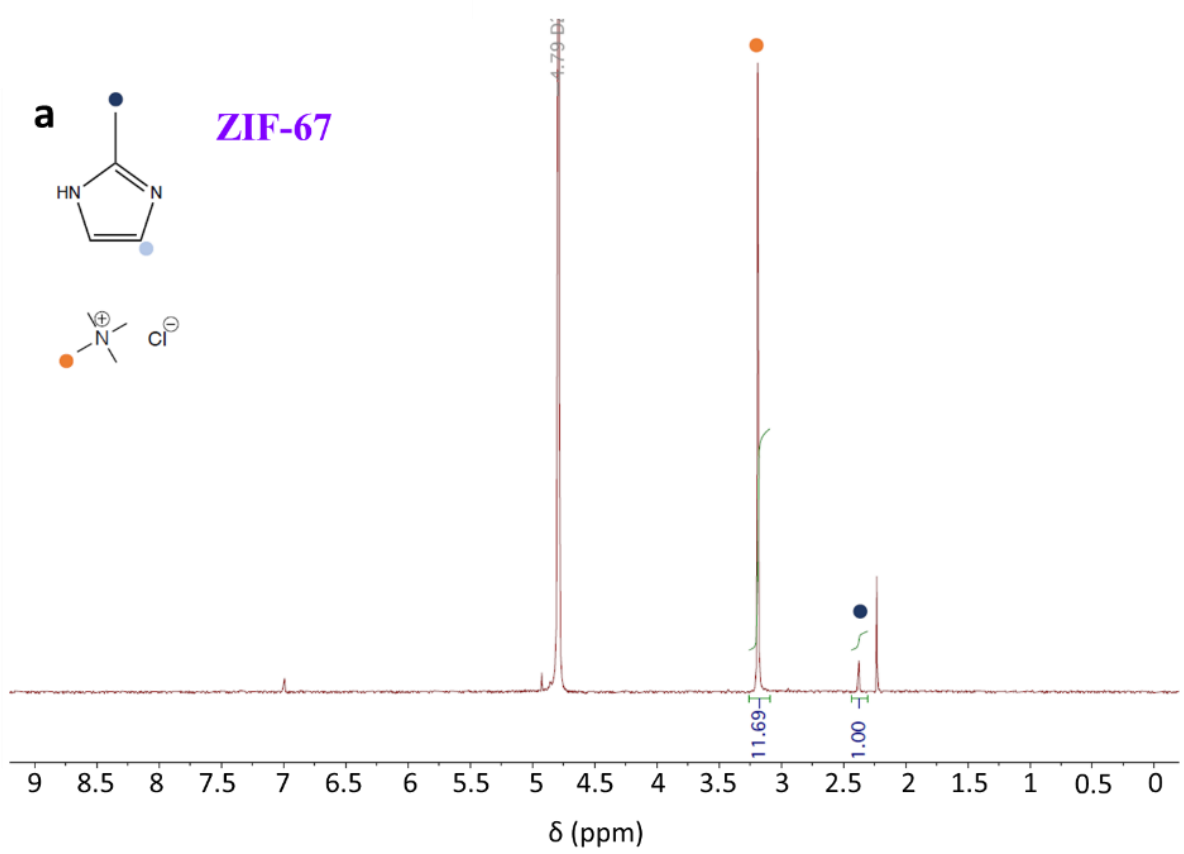
a
ZIF-67
HN
N
N
Cl
4.79
11.69
1.00
9 8.5 8 7.5 7 6.5 6 5.5 5 4.5 4 3.5 3 2.5 2 1.5 1 0.5 0
δ (ppm)

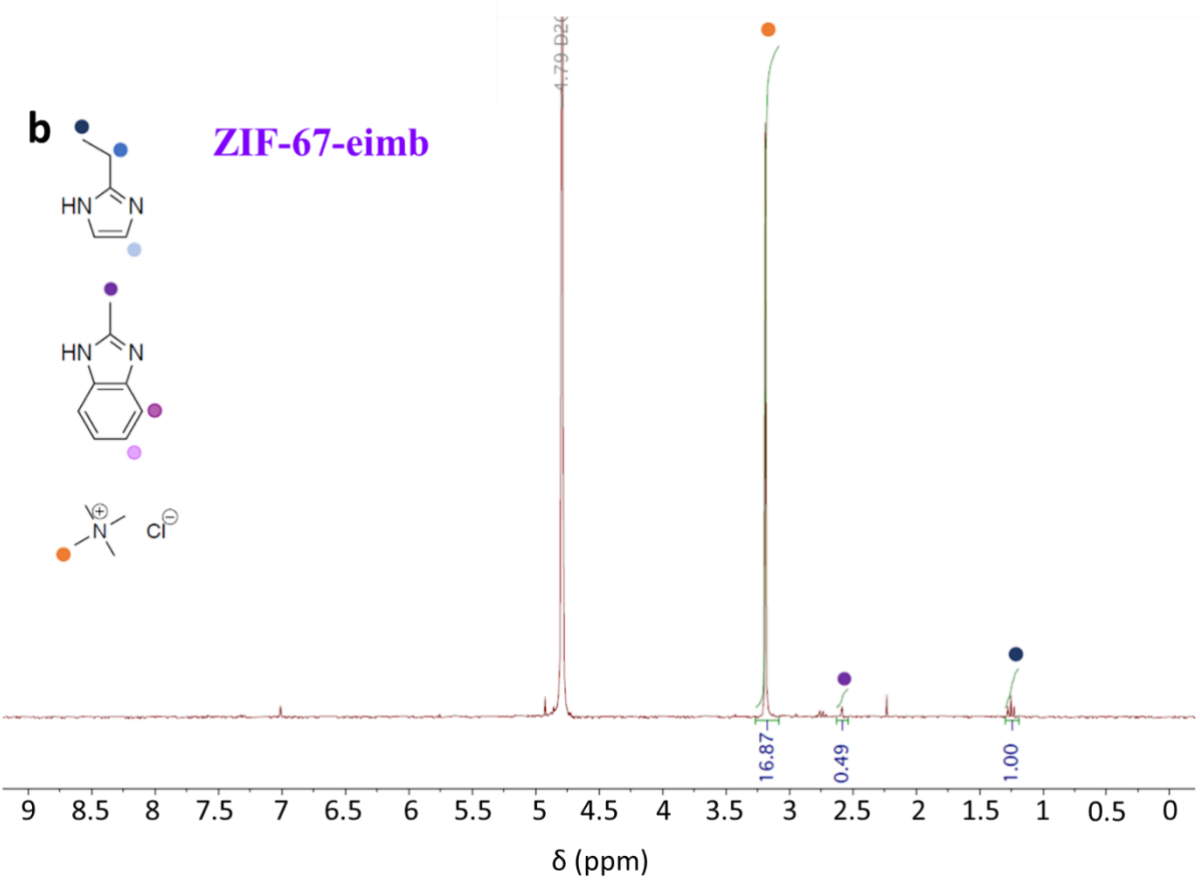
b
ZIF-67-eimb
HN
N
HN
N
N
Cl
4.79
16.87
0.49
1.00
9 8.5 8 7.5 7 6.5 6 5.5 5 4.5 4 3.5 3 2.5 2 1.5 1 0.5 0
δ (ppm)

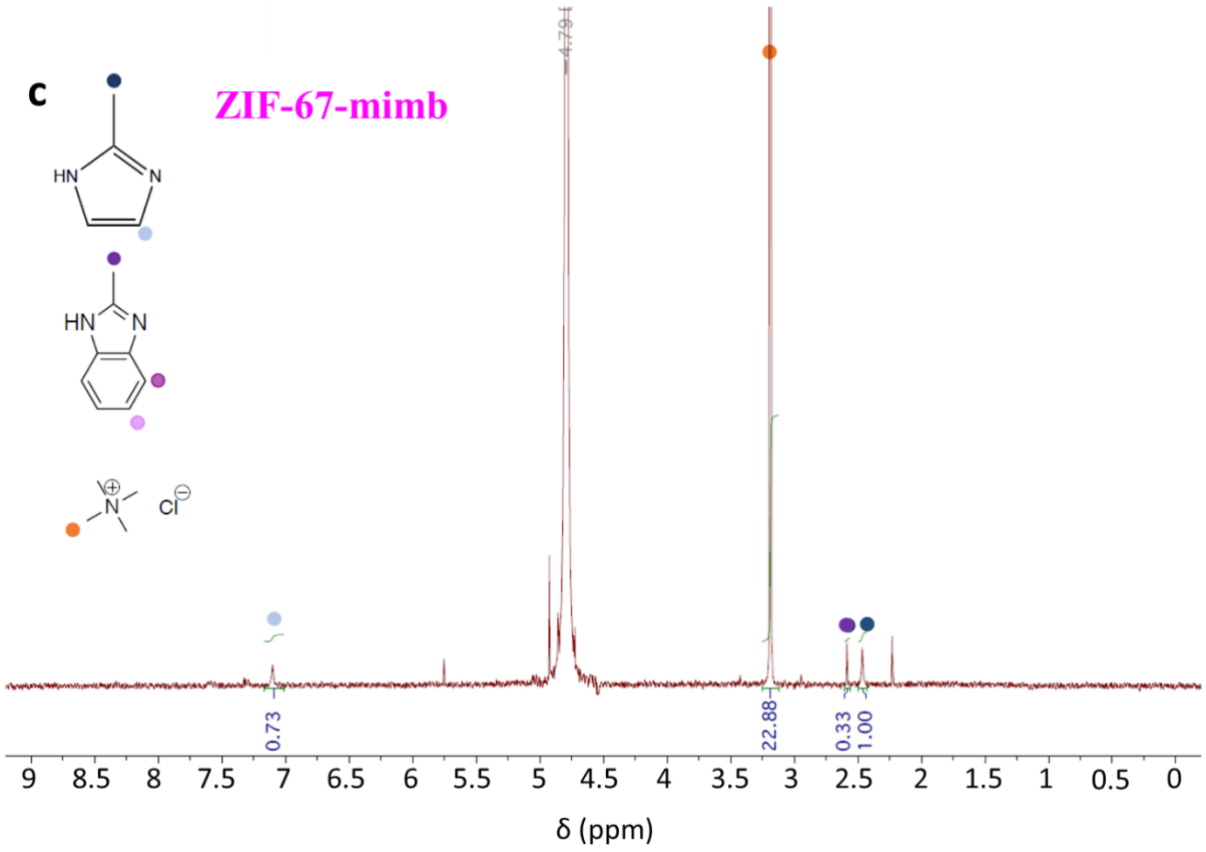

Figure S31. NMR spectra of **ZIF-67** (a), **ZIF-67-eimb** (b) and **ZIF-67-mimb** (c). Coloured circles help to localize the corresponding chemical shifts of the protons

S4.3 Contact angle measurements

Static water contact angle measurements of samples **ZIF-67**, **ZIF-67-eimi, ZIF-67-eimb** and **ZIF-67-mimb** were performed in air using a Rame-hart 200 standard goniometer equipped with an automated dispensing system. The initial drop volume was 0.25 μL, increased by additions of 0.25 μL.

ZIF-67 has a contact angle value to 120º, although the size of the water is limited to 1.00 μL (the drop is adsorbed upon further addition). Inclusion of 2-ethylimidazole causes an increase in the contact angles to 145 °, whereas inclusion of 2-methylbenzimidazole causes an increase in the contact angle values to 132 °, thus showing an increase in the hydrophobic character. In these cases, the final drop volume can be as high as 2.25 μL.

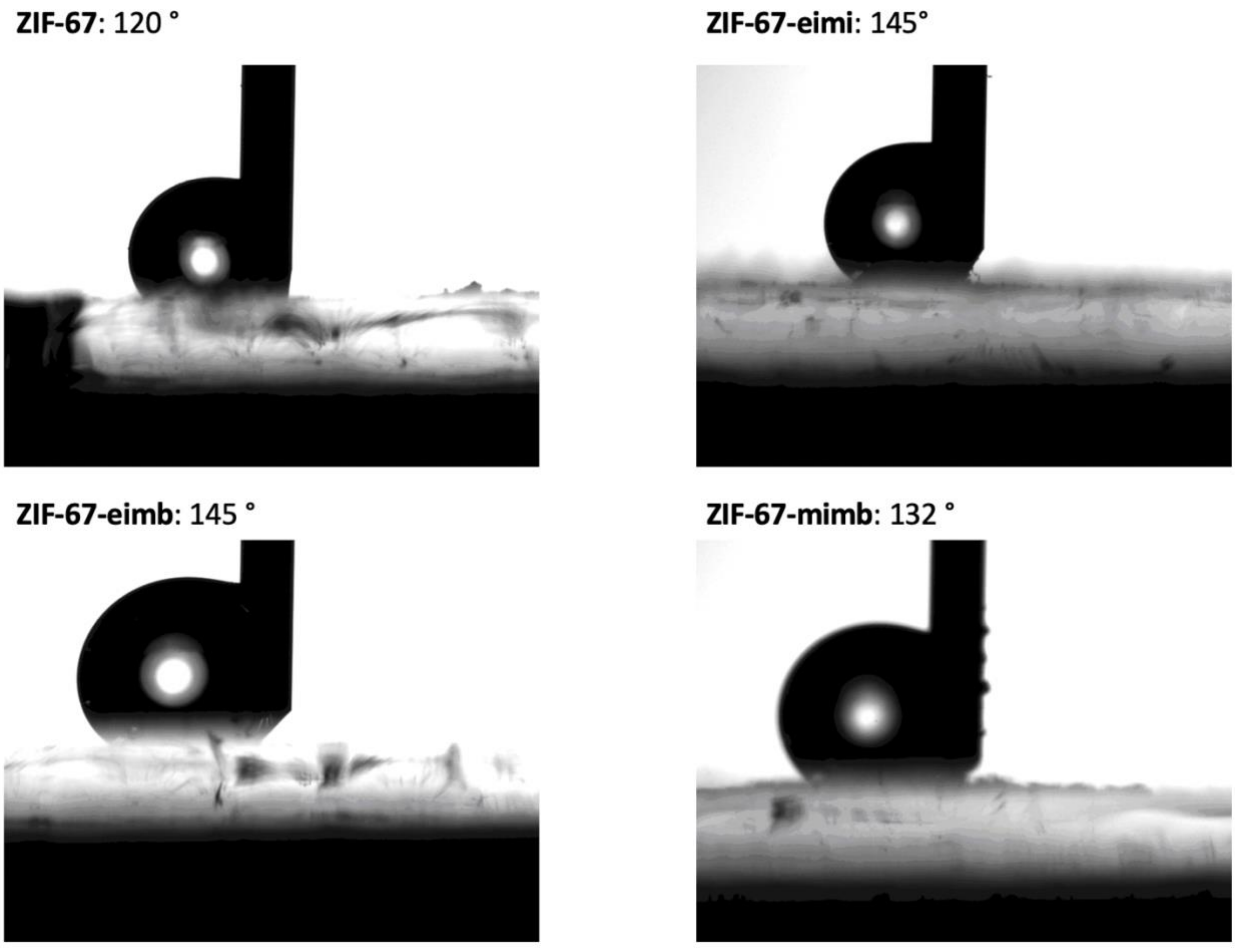

Figure S32. Surface modification in **ZIF-67** (a), **ZIF-67-eimb** (b) and **ZIF-67-mimb**. The use of different mixtures of ligands causes different surface behaviors which change the water contact angle.

S5 References

(1) López-Cabrelles, J.; Romero, J.; Abellán, G.; Giménez-Marqués, M.; Palomino, M.; Valencia, S.; Rey, F.; Mínguez Espallargas, G. *J. Am. Chem. Soc.* 2019, **141** (17), 7173–7180.

(2) Dolomanov, O. V.; Bourhis, L. J.; Gildea, R. J.; Howard, J. A. K.; Puschmann, H.*J. Appl. Crystallogr.* 2009, **42** (2), 339–341.

(3) Sheldrick, G. M. *Acta Crystallogr. Sect. C Struct. Chem.* 2015, **71** (1), 3–8.

(4) Fisher, M. E. *Philos. Mag.* 1962, **7** (82), 1731–1743.

(5) Blum, V.; Gehrke, R.; Hanke, F.; Havu, P.; Havu, V.; Ren, X.; Reuter, K.; Scheffler, M.. *Comput. Phys. Commun.* 2009, **180** (11), 2175–2196.

(6) Perdew, J. P.; Ruzsinszky, A.; Csonka, G. I.; Vydrov, O. A.; Scuseria, G. E.; Constantin, L. A.; Zhou, X.; Burke, K. *Phys. Rev. Lett.* 2008, **100** (13), 136406.

(7) Zhang, I. Y.; Ren, X.; Rinke, P.; Blum, V.; Scheffler, M. *New J. Phys.* 2013, **15** (12), 123033.

(8) Tkatchenko, A.; Scheffler, M. *Phys. Rev. Lett.* 2009, **102** (7), 073005.

(9) Chemcraft - graphical software for visualization of quantum chemistry computations.

https://www.chemcraftprog.com

(10) Momma, K.; Izumi, F. *J. Appl. Crystallogr*. 2011, **44** (6), 1272–1276.

(11) Zhang, H.; Zhao, M.; Lin, Y. S. *Microporous Mesoporous Mater*. 2019, **279**, 201–210.

(12) Zhang, Y.; Jia, Y.; Li, M.; Hou, L. *Sci. Rep.* 2018, **8** (1), 1–7.

(13) Stassin, T.; Stassen, I.; Marreiros, J.; Cruz, A. J.; Verbeke, R.; Tu, M.; Reinsch, H.; Dickmann, M.; Egger, W.; Vankelecom, I. F. J.; De Vos, D. E.; Ameloot, R. *Chem. Mater*. 2020, **32** (5), 1784–1793.